arXiv:1409.5304v1 [cond-mat.soft] 18 Sep 2014

Accurate coarse-grained models for mixtures of colloids and linear polymers under good-solvent conditions.

Giuseppe D'Adamo*
SISSA, V. Bonomea 265, I-34136 Trieste, Italy

Andrea Pelissetto†
Dipartimento di Fisica, Sapienza Università di Roma and INFN, Sezione di Roma I, P.le Aldo Moro 2, I-00185 Roma, Italy

Carlo Pierleoni‡
Dipartimento di Scienze Fisiche e Chimiche, Università dell'Aquila and CNISM, UdR dell'Aquila, V. Vetoio 10, Loc. Coppito, I-67100 L'Aquila, Italy

(Dated: September 19, 2014)

A coarse-graining strategy, previously developed for polymer solutions, is extended here to mixtures of linear polymers and hard-sphere colloids. In this approach groups of monomers are mapped onto a single pseudoatom (a blob) and the effective blob-blob interactions are obtained by requiring the model to reproduce some large-scale structural properties in the zero-density limit. We show that an accurate parametrization of the polymer-colloid interactions is obtained by simply introducing pair potentials between blobs and colloids. For the coarse-grained model in which polymers are modelled as four-blob chains (tetramers), the pair potentials are determined by means of the iterative Boltzmann inversion scheme, taking full-monomer pair correlation functions at zero-density as targets. For a larger number n of blobs, pair potentials are determined by using a simple transferability assumption based on the polymer self-similarity. We validate the model by comparing its predictions with full-monomer results for the interfacial properties of polymer solutions in the presence of a single colloid and for thermodynamic and structural properties in the homogeneous phase at finite polymer and colloid density. The tetramer model is quite accurate for $q \lesssim 1$ ($q = \hat{R}_g/R_c$, where $\hat{R}_g$ is the zero-density polymer radius of gyration and R_c is the colloid radius) and reasonably good also for $q = 2$. For $q = 2$ an accurate coarse-grained description is obtained by using the $n = 10$ blob model. We also compare our results with those obtained by using single-blob models with state-dependent potentials.

PACS numbers: 61.25.he, 65.20.De, 82.35.Lr

I. INTRODUCTION

Colloid dispersions are systems of great interest in several areas, because of their complex behavior and their many technological applications. Their phase behavior depends in a sensitive way on the range of the colloid-colloid attraction relative to the colloid size. In the presence of very short-range interactions only fluid-solid coexistence occurs, as is the case for the hard-sphere fluid. As the range of the attraction is increased, a fluid-fluid transition can also occur. The addition of nonadsorbing neutral polymers to a colloidal dispersion provides an easy method to modify in a controlled fashion the range of the attractive effective force between the colloids, hence it allows one to modify at will the phase behavior of the system. For dispersions of spherical colloids and (sufficiently long) nonadsorbing neutral polymers in an organic solvent, phase behavior depends[1–7] to a large extent only on the nature of the solvent and on the ratio $q \equiv \hat{R}_g/R_c$, where $\hat{R}_g$ is the zero-density radius of gyration of the polymer and R_c is the radius of the colloid. If q is smaller than a critical value q_{CEP}, only fluid-solid coexistence occurs, while in the opposite case there is also a fluid-fluid coexistence of a colloid-rich, polymer-poor phase (colloid liquid) with a colloid-poor, polymer-rich phase (colloid gas). Extensive theoretical and experimental work predict[1] $q_{CEP} \approx 0.3$-0.4 for polymers under good-solvent conditions.

Several approaches have been used to determine the phase diagram of colloid-polymer mixtures. On one side, several approximate thermodynamic approaches have been used. We mention the PRISM approach,[8–10] density functional theory,[11,12] and thermodynamic perturbation theory.[13,14] Another successful approach is free-volume theory[15] which has been originally developed for mixtures of colloids and ideal polymers and later generalized to include polymer-polymer and polymer-colloid interactions.[6,16–19] Such an approach appears to be quite accurate[6,19,20] as long as $q \lesssim 1$. Numerical simulations of colloid-polymer systems have also been performed. Simulations using full-monomer representations of the polymers[21–24] are difficult, because of the large number of degrees of freedom involved. As a consequence, the simulated chains are typically relatively short. This implies that results are affected by significant corrections to scaling, which must be taken into account before comparing them with experimental data or with results obtained in other approaches (see Ref. 20 for a discussion). To avoid these difficulties, coarse-grained (CG) approaches have

been developed. In these models, short-scale degrees of freedom of the polymer subsystem are integrated out, providing a simpler representation of the polymers that still allows one to obtain accurate results for the thermodynamics of the system and for large-scale (i.e., on length scales comparable to the polymer size) structural properties in some range of densities and of polymer-to-colloid size ratios. Beside the obvious advantage from the computational side, CG models are also very convenient since they provide directly thermodynamics and structural properties in the universal, scaling limit without requiring additional extrapolations. For this purpose it is enough to determine the target properties on which the CG model is built in the scaling limit.

Several CG models have been introduced for polymer solutions in different concentration regimes.[25–36] In the simplest approaches (single-blob representations), one maps polymer chains onto point particles interacting by means of spherically symmetric potentials.[25–27] In the good-solvent regime, models with density-independent potentials, i.e., obtained at zero polymer density, reproduce the thermodynamic behavior of polymer solutions up to polymer volume fractions ϕ_p of order 1 ($\phi_p = 4\pi \hat{R}_g^3 \rho_p/V$, where ρ_p is the polymer number density and V is the volume), i.e., as long as polymer-polymer overlaps are rare, so that the neglected many-body interactions[37] are not relevant. These simple models have been extended to include polymer-colloid interactions.[38–44] For colloid-polymer systems, these approaches are generically expected to be predictive only in the colloid regime $q \lesssim 1$. Indeed, for $q \gtrsim 1$, corresponding to $\hat{R}_g \gtrsim R_c$, the polymer can wrap around the colloid, making the monoatomic (single-blob) approximation for the polymers unrealistic.

Single-blob models with potentials dependent on the polymer density have also been considered.[26,27,45] Such models, by definition, reproduce some large-scale properties of the system for all values of ϕ_p in the limit of zero colloidal density. In this approach, however, there are several sources of ambiguity. First, potentials do not only depend on the state point one considers, but also on the chosen ensemble,[46] i.e., on the thermodynamic variable (for instance, the density or the chemical potential) chosen to specify the thermodynamic state point. Moreover, also the determination of the thermodynamic properties is ambiguous, since different approaches, which are equivalent for systems with state-independent interactions, provide different results for the same quantity.[46–48] Since potentials are not allowed to depend on the colloidal density ρ_c, for finite ρ_c this approach only provides an approximation to the correct behavior, with the same limitations of the simpler zero-density single-blob approach. In particular, also this class of single-blob models is expected to be predictive only for $q \lesssim 1$.

These limitations can be overcome by switching to a model at a lower level of coarse graining: A long polymer chain is mapped onto a short chain of n soft monomers (blobs).[28,30,31] For purely polymeric systems, these CG models predict the correct thermodynamic and large-scale structural properties of the solution as long as blob overlaps are rare.[28,31] In the semidilute regime this condition is satisfied for $\hat{r}_g \ll \xi$, where $\hat{r}_g$ is the zero-density blob radius of gyration and ξ is the de Gennes correlation length, which is the only relevant length scale in the semidilute regime. Since[30] $\hat{r}_g/\hat{R}_g \sim n^{-\nu}$ and[49] $\xi/\hat{R}_g \sim \phi_p^{-\gamma}$, where $\gamma = \nu/(3\nu-1)$ and ν is the Flory exponent ($\nu = 0.587597(7) \approx 3/5$, see Ref. 50), the condition $\hat{r}_g \ll \xi$ is equivalent to $\phi_p \lesssim n^{3\nu-1} \approx n^{0.76}$ under good-solvent conditions. Therefore, by increasing the number n of blobs, the CG model becomes predictive in a larger density interval. Analogously, in the presence of colloids, the pairwise approximation in which many-body interactions are neglected only holds if $\hat{r}_g/R_c \lesssim 1$, i.e., for $q \lesssim n^{\nu}$. This condition guarantees that the average distance between two colloids is larger than $\hat{r}_g$ and that, therefore, only pair interactions are relevant. Again, by increasing the number n of blobs we can extend the validity of CG models to larger values of q.

Recently, we have introduced a procedure to set up a hierarchy of CG models for linear polymer chains under good-solvent conditions which simultaneously reproduce quite accurately structure and thermodynamics of polymer solutions deep into the semidilute regime.[30,31] We followed the structure-based route[51–55] (an alternative, conceptually different approach is the force-matching route, discussed, e.g., in Refs. 56,57), in which the CG model is set up in such a way to reproduce full-monomer correlation functions of a set of chosen structural collective variables, which are determined at zero polymer density. Since simulations of a few isolated polymer chains are relatively easy, we were able to obtain the target correlation functions for polymer chains of several lengths with high numerical precision. Therefore, we could perform a reliable extrapolation to obtain target properties in the scaling, universal limit. This guarantees that the CG model gives thermodynamical and structural predictions in the scaling limit, which can directly be compared with experiments on high-molecular-weight polymers.

In the minimal model each linear chain is represented by a short polyatomic molecule with four sites (tetramer). The tetramer potentials are set up at zero density—this allows us to avoid the inconsistencies[46–48] that occur when using state-dependent potentials—by matching the single-chain intramolecular structure and the center-of-mass pair correlation function between two identical chains. This minimal representation has been shown to provide accurate results for the underlying solutions up to $\phi_p \simeq 2$.[30] Higher-resolution models with $n > 4$ are obtained by using a simple transferability approach, which allows one to obtain the interaction potentials for n blob systems starting from those computed for the tetramer. This transferability approximation, extensively discussed in Sec. V.A of Ref. 58, was shown to be quite accurate[31] and allowed us to obtain precise thermodynamic and (large-scale) structural results for $\phi_p \gg 1$. For instance, the multiblob CG models predict the isothermal com-

pressibility with an error of less then 10% up to $\phi_p \approx 2$ for $n = 4$, $\phi_p \approx 4.5$ for $n = 10$ and up to $\phi_p \approx 10$ for $n = 30$.

In this paper we extend the multiblob approach to colloid-polymer mixtures. Colloids are modelled as hard spheres of radius R_c, while a multiblob model is used for polymers. First, we consider the case in which each polymer is represented by a four-blob (tetramer) CG molecule. The resulting CG model, in which polymer-colloid interactions are simply approximated by pair potentials between the blobs and the hard sphere, works quite well up to $q \approx 2$ in the homogeneous phase and represents a significant improvement with respect to the single-blob case. Then, we extend the model to $n > 4$ by using a simple transferability argument, analogous to that presented in Ref. 31. To validate the model, we compare the numerical data obtained by using the CG models with full-monomer simulation results for $q = 0.5$, 1, and 2. Beside being of relevance for the test of the CG model, these simulations also provide new results for the intermolecular and intramolecular structure in a colloidal dispersion.

The paper is organized as follows. In Sec. II we define our basic CG model in which each polymer is represented by a four-blob (tetramer) CG molecule. In Sections III, IV, and V we determine the accuracy with which the tetramer model reproduces the behavior of the polymer-colloid mixture. First, we consider the third virial coefficients, that allow us to estimate how large the neglected three-body effects are.[59,60] Then, we consider the behavior of a single colloid in a bath of polymers. In Sec. V we present full-monomer results in the homogeneous phase for $q = 0.5$, $q = 1$ and $q = 2$. We determine several thermodynamic quantities, which are then compared with the corresponding tetramer results. In Sec. VI we consider the transferability in the number of blobs, determining a decamer model, which is validated by using the full-monomer results derived in the preceding sections. In Sec. VII we discuss single-blob models with state-dependent interactions, generalizing that proposed in Ref. 26,27,37,40. Finally, in Sec. VIII we draw our conclusions. In App. A we collect some formulae that are useful to determine some thermodynamic quantities from Monte Carlo estimates of the partial structure factors. In App. B we discuss the polymer and blob size in the homogeneous phase as a function of ϕ_c and ϕ_p. In App. C we explain how to determine state-dependent single-blob potentials in the grand-canonical ensemble by using integral-equation methods. Details are collected in the supplementary material.[61] We define the polymer model we use to compute full-monomer properties, we give interpolations of the colloid-blob potentials determined for the tetramer model (for the pure polymer system, see the supplementary material of Ref. 58), and provide extensive tables of thermodynamic data in the homogeneous phase.

II. THE COARSE-GRAINED MODEL

A. Definitions

In the multiblob approach one starts from a *coarse-grained representation* (CGR) of the underlying full-monomer model, which is obtained by mapping a chain of L monomers onto a chain of n blobs, each of them located at the center of mass of a subchain of $m = L/n$ monomers. If the monomer positions are given by $\{\mathbf{r}_1, \ldots, \mathbf{r}_L\}$, one first defines the blob positions $\mathbf{s}_1, \ldots, \mathbf{s}_n$ as the centers of mass of the subchains of length m, i.e.

$$\mathbf{s}_i = \frac{1}{m} \sum_{\alpha=m(i-1)+1}^{mi} \mathbf{r}_\alpha. \tag{1}$$

For the new CG chain $\{\mathbf{s}_1, \ldots, \mathbf{s}_n\}$ one defines several intramolecular and intermolecular correlation functions, which are then used as target properties for the definition of the CG model.

The CG model consists of polyatomic molecules of n atoms located in $\{\mathbf{t}_1, \ldots, \mathbf{t}_n\}$. All length scales are expressed in terms of the full-monomer zero-density radius of gyration $\hat{R}_g$, hence all potentials and distribution functions depend on the adimensional combinations $\mathbf{b} = \mathbf{t}/\hat{R}_g$. As discussed in Ref. 30, it is not feasible to reproduce exactly the structure of the full-monomer model, even at the CGR level, since this would require the introduction of complex many-body interactions. However, a judicious parametrization of the interactions in terms of pair potentials, each of them depending on a single scalar variable, works quite well.[30] In this paper we apply the same strategy to polymer-colloid mixtures, determining the appropriate effective intermolecular interactions between polymer blobs and colloids. In the spirit of the multiblob approach, we neglect interactions among three or more molecules and consider only the interaction between a polymer and a colloid. In general, it depends on $3(n-1)$ scalar variables, parametrizing the relative position of the blobs and of the colloid. The exact determination of this many-body potential is, of course, unfeasible in practice. Therefore, we make a pair-potential approximation. The polymer-colloid interaction is completely specified by the blob-colloid pair potentials $V_{cp,i}(b, q)$, where i is the blob index along the chain, $b = |\mathbf{r}_c - \mathbf{t}_i|/\hat{R}_g$, and $\mathbf{r}_c$, $\mathbf{t}_i$ are the colloid and blob positions, respectively. Note that the potentials depend on q, which is explicitly reported in the notation.

As in Ref. 30, we begin by considering the tetramer case $n = 4$. For this value of n there are two independent potentials $V_{cp,1}(b, q) = V_{cp,4}(b, q)$ and $V_{cp,2}(b, q) = V_{cp,3}(b, q)$. They are determined by requiring the CG model to reproduce the distribution functions $g_{cp,i}(b, q)$ between the center of mass of blob i and the colloid, where $r = |\mathbf{r}_c - \mathbf{s}_i|$ and $b = r/\hat{R}_g$. For $n > 4$ a direct computation of the potentials is unfeasible, hence we will use a simple transferability approach as in Ref. 31.

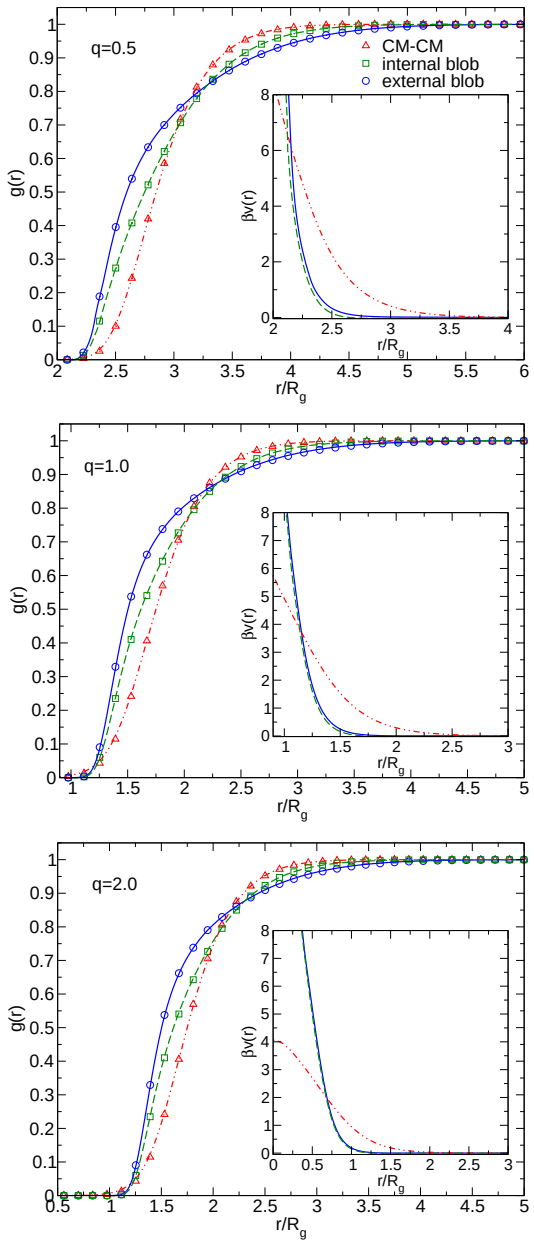

FIG. 1: Pair distribution functions between the centers of mass of the blobs and the colloid (solid lines and circles refer to the external blobs, dashed lines and squares to the internal blobs) and between the center of mass of the polymer and the colloid (dash-dot-dot line and triangles). Symbols refer to the CG estimates, while the lines are the corresponding full-monomer results. In the inset the corresponding potentials are shown with the same line conventions as for the distribution functions. Results for $q = 0.5$ (top), 1 (middle), and 2 (bottom).

B. Tetramer polymer model

In order to determine full-monomer properties, we consider the three-dimensional lattice Domb-Joyce model[62] as in our previous work (see the supplementary material[61] for the precise definition). In the absence of colloids, there is a significant advantage in using Domb-Joyce chains instead of other models. For a generic polymer model, the leading scaling corrections decay slowly, as $L^{-\Delta}$ ($\Delta = 0.528(12)$, Ref. 50), where L is the number of monomers of each chain. Therefore, the universal, large–degree-of-polymerization limit is only observed for quite large values of L. On the other hand, if the repulsion parameter that appears in the Domb-Joyce Hamiltonian is chosen appropriately, the scaling corrections decay faster, approximately as $1/L$.[63,64] As a consequence, scaling results are obtained by using significantly shorter chains (for zero-density quantities, simulations of chains with 600 monomers give results that are essentially asymptotic). Unfortunately, in the presence of a repulsive surface, new renormalization-group operators arise, which are associated with the surface.[65] The leading one gives rise to corrections that scale as $L^{-\nu}$,[65] where ν is the Flory exponent (an explicit test of this prediction is presented in the supplementary material of Ref. 66), hence it spoils somewhat the nice scaling behavior observed in the absence of colloids. These corrections are not negligible, even for chain lengths of the order of 10^3. Therefore, finite-length polymer-colloid results must be extrapolated to obtain scaling results.

In practice, we work as follows. We consider Domb-Joyce chains of length $L = 240$, $L = 600$, and $L = 2400$. For each value of q and L we determine the blob-colloid distribution functions $g_{cp,i}(r, L, q)$ by Monte Carlo simulations. In the scaling limit $L \to \infty$, these quantities converge to universal functions, once distances are expressed in units of the size of the polymer, i.e., in terms of the adimensional ratio $b = r/\hat{R}_g$. Therefore, for each L we interpolate $g_{cp,i}(b, L, q)$ by means of a cubic spline. Then, the data for the three values of L are extrapolated by assuming $g_{cp,i}(b, L, q) = a(b, q) + c(b, q)L^{-\nu} + d(b, q)/L$. Solving the simple linear system, we obtain $a(b, q)$ and set $g_{cp,i}(b, q) = a(b, q)$. This quantity is then used as target distribution function.

Once the target functions are known, the potentials are obtained by applying the Iterative Boltzmann Inversion (IBI) scheme.[51,52,67] Less than ten iterations are needed to reproduce the target quantities quite precisely. In Fig. 1 we show the blob-colloid pair distribution functions and the corresponding effective potentials for the tetramer for three values of the size ratio, $q = 0.5, 1.0, 2.0$. The potentials are short ranged and become very small approximately for $r/\hat{R}_g \approx 1/q + 0.5$. This is consistent with the idea that the typical range is of the order of $R_c + \hat{r}_g$, since $\hat{r}_g \approx 0.45\hat{R}_g$ for a tetramer.[30] Moreover, they increase steeply as b approaches the contact point $R_c/\hat{R}_g = 1/q$. For $q = 0.5$ and 1, colloids and blobs cannot approach each other by less than R_c and indeed, the potentials apparently diverge when $b \to 1/q$. On the other hand, for $\hat{r}_g \gtrsim R_c$ the blobs can wrap around the colloids, hence there is a finite probability that the distance between the blob and the colloid is less than R_c.

This occurs for $q = 2$ (we have[30] $\hat{r}_g \approx 0.95 R_c$ in this case). For this value of q, $\beta V_{cp,i}(1/q, 2) \approx 5$.

The difference between the potentials associated with the internal and external blobs—the internal-blob potential is less repulsive than the external one—is small but not negligible, especially for $q = 0.5$, and decreases with q. An attractive tail of the order of $10^{-2} k_B T$ is also observed but we believe it is a numerical artifact of the IBI procedure, as reported in other contexts.[51]

III. COMPARISON OF FULL-MONOMER AND TETRAMER RESULTS AT ZERO-DENSITY

We wish now to discuss the behavior of the CG model in the thermodynamic regime in which both the colloidal and the polymer densities $\rho_p = N_p/V$ and $\rho_c = N_c/V$ are small. In this limit the thermodynamic properties of interest can be expressed as a series expansion in the concentration variables. The coefficients of these expansions can be typically related to the virial coefficients parametrizing the concentration dependence of the (osmotic) pressure P. At third order in the densities we have

$$\beta P \approx \rho_c + \rho_p + B_{2,cc}\rho_c^2 + B_{2,cp}\rho_c\rho_p + B_{2,pp}\rho_p^2 + B_{3,ccc}\rho_c^3 + B_{3,ccp}\rho_c^2\rho_p + B_{3,cpp}\rho_c\rho_p^2 + B_{3,ppp}\rho_p^3 \quad (2)$$

Although virial coefficients are model dependent, their adimensional combinations $A_{2,\#} = B_{2,\#}\hat{R}_g^{-3}$ and $A_{3,\#} = B_{3,\#}\hat{R}_g^{-6}$ are universal. Hence, it makes sense to compare full-monomer predictions with CG results. Since the CG model has been defined by matching the blob-colloid distribution functions, the compressibility rule[68] implies that $A_{2,cp}$ should be the same in the full-monomer and in the CG model. Hence, the comparison of $A_{2,cp}$ allows us to verify the accuracy of the inversion procedure. Results for $A_{2,cp}$ are reported in Table I.[69] In all cases $A_{2,cp}$ is close to the full-monomer estimate, confirming the validity of the CG potentials. The comparison of the estimates of the third-virial combinations is much more interesting, since it allows us to estimate how effective the CG model is in modelling three-body interactions,[59,60] which are relevant in the concentration regimes in which multiple overlaps between polymers and colloids cannot be neglected.

In Table I we collect results for the third-virial combinations obtained from full-monomer simulations[66] and for the CG model at various levels of resolution. For future convenience, we also present results for the CG model with $n = 10$ blob, the decamer, a CG model that will be discussed in Sec. VI (the same comment applies to the Tables and figures that will be presented below). As it was shown in Ref. 66, App. A, for polyatomic molecules these quantities are the sum of two contributions. One contribution, that we denote with $A^I_{3,\#}$ is the usual term that gives the third virial coefficient in simple liquids of monatomic molecules (diagramatically, it is associated with the triangle diagram[68]). The second contribution, denoted with $A^{\rm fl}_{3,\#}$, is a flexibility contribution that takes into account the conformational properties of the polymers. It represents a small, but not negligible correction to $A^I_{3,\#}$, which becomes more important as q increases. Both quantities are universal, hence a separate comparison is meaningful.

As already observed in the purely polymeric case,[30] the tetramer model reproduces well the third virial combinations, indicating that three-body interactions are correctly taken into account, at least up to $q \approx 2$. The relative difference between the tetramer and full-monomer estimates of $A_{3,ppc}$ is 1% and 2% for $q = 1$ and $q = 2$, respectively. Similar observations hold for $A_{3,ccp}$ that is accurately reproduced by the CG model: differences are at most of 0.3% and 1.5% for $q = 1$ and $q = 2$, respectively. Note that the three-body effects involving two colloids and one polymer are better reproduced than those involving two polymers and one colloid. The data of Table I also show that the tetramer represents a significant improvement with respect to the single-blob model. First, the latter is unable to reproduce the flexibility correction. Second, deviations from the correct, full-monomer results are quite significant: $A_{3,ccp}$ and $A_{3,cpp}$ are underestimated by 10% and 5% for $q = 1$, respectively. For $q = 2$ deviations are significantly larger: $A_{3,cpp}$ differs by a factor of two from the full-monomer result.

As an additional check of the validity of the procedure we have compared the distribution function $g_{cp,CM}(b, q)$ between the colloid and the polymer center of mass computed in the full-monomer and in the CG model. Since we used the blob-colloid distribution functions as targets for the inversion procedure, this is a nontrivial check that allows us to verify how good the pair-potential approximation is for the intermolecular interactions. The results are shown in Fig. 1. In all cases, we observe a very good agreement, confirming the accuracy of the procedure.

IV. FULL-MONOMER AND TETRAMER RESULTS FOR A PURE POLYMER SOLUTION IN THE PRESENCE OF A SPHERICAL SOLUTE

Let us now compare the tetramer and the full-monomer results for generic values of ϕ_p and vanishing colloidal density. For this purpose we consider the solvation properties of a single colloid in the polymer solution. The relevant quantity here is the insertion free energy, which gives the free energy change due to the insertion of a colloid at fixed polymer chemical potential. Equivalently, one can use the depletion thickness δ_s, which represents the average width of the depleted layer around the colloid.[6,17,19,70]

Such a quantity can be related to the integral of any polymer-colloid distribution function. For instance, if $g_{{\rm mon},cp}(\mathbf{r}; \mu_p)$ and $g_{cp,i}(\mathbf{r}; \mu_p)$ are the monomer-colloid and blob-colloid distribution functions at a given poly-

TABLE I: Virial combinations for full-monomer (FM) systems (scaling-limit values from Ref. 66), for the single-blob model ($n = 1$), for the tetramer ($n = 4$), and for the decamer ($n = 10$, method c)). For the third-virial combinations, we also report the simple-liquid contribution $A^I_{3,\#}$ and the flexibility contribution $A^{\rm fl}_{3,\#}$ (see Ref. 66, App. A, for the definitions): $A_{3,\#} = A^I_{3,\#} + A^{\rm fl}_{3,\#}$.

q	n	$A_{2,cp}$	$A^I_{3,cpp}$	$A^{\rm fl}_{3,cpp}$	$A_{3,cpp}$	$A^I_{3,ccp}$	$A^{\rm fl}_{3,ccp}$	$A_{3,ccp}$
0.5	FM	107.4(3)	748(4)	−22(2)	726(5)	8759(45)	−130(6)	8630(45)
	1	107.253(6)	704.7(4)	0	704.7(4)	8621(2)	0	8621(2)
	4	107.49(3)	757.7(6)	−16(1)	742(2)	8771(14)	−120(6)	8651(13)
1	FM	27.54(6)	140.0(8)	−6.8(2)	133.3(9)	371(2)	−12.2(5)	360(2)
	1	27.289(2)	119.53(8)	0	119.53(8)	340.6(2)	0	340.6(2)
	4	27.70(1)	140.0(5)	−4.8(4)	135.3(6)	370(2)	−10.6(6)	359(2)
	10	27.592(7)	143.6(2)	−6.0(2)	137.6(3)	374.9(4)	−11.8(4)	363.1(4)
2	FM	8.65(5)	28.1(2)	−2.0(1)	26.1(2)	17.80(2)	−1.03(5)	16.8(1)
	1	8.6049(9)	13.25(3)	0	13.25(3)	20.36(2)	0	20.36(2)
	4	8.679(3)	27.3(1)	−1.3(1)	26.0(2)	17.4(2)	−0.81(6)	16.6(2)
	10	8.687(5)	28.8(1)	−1.8(2)	27.0(3)	18.0(1)	−0.8(1)	17.0(2)

TABLE II: Depletion thickness $\delta_s(\phi_p)/R_c$ as a function of the polymer volume fraction ϕ_p. Full-monomer (FM), single-blob ($n = 1$), tetramer ($n = 4$), and decamer ($n = 10$) results.

q	ϕ_p	FM	$n = 1$	$n = 4$	$n = 10$
0.5	0.0	0.474(1)	0.47371(2)	0.4745(1)	
	0.4	0.335(25)	0.326(2)	0.333(1)	
	1.0	0.239(6)	0.215(2)	0.239(3)	
	2.0	0.168(5)	0.118(3)	0.166(4)	
1.0	0.0	0.873(41)	0.86767(5)	0.8764(3)	0.8745(2)
	0.4	0.624(17)	0.586(4)	0.62(2)	0.61(1)
	1.0	0.436(11)	0.384(3)	0.43(1)	0.44(1)
	2.0	0.335(45)	0.205(2)	0.30(1)	0.315(6)
2.0	0.0	1.547(2)	1.54243(9)	1.5487(3)	1.5501(5)
	0.4	1.10(8)	1.045(20)	1.08(1)	1.10(1)
	1.0	0.795(25)	0.721(5)	0.780(9)	0.788(6)
	2.0	0.65(8)	0.43(5)	0.532(9)	0.54(1)

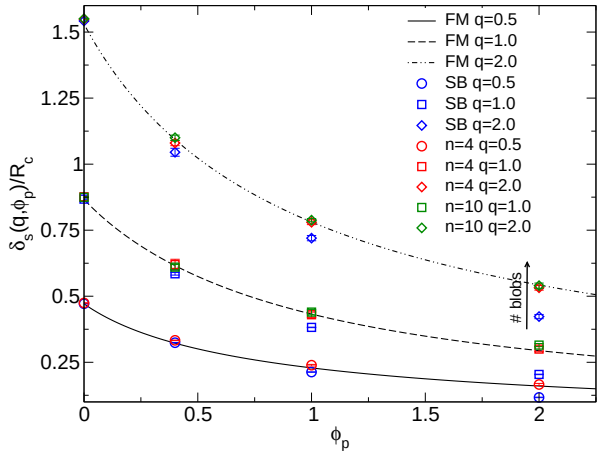

FIG. 2: Depletion thickness versus ϕ_p. Full-monomer (lines, FM, from Ref. 66), single-blob (SB), tetramer ($n = 4$), and decamer ($n = 10$) results.

mer chemical potential μ_p, the integral $G_{cp}(\mu_p)$ defined by

$$G_{cp}(\mu_p) = \int d\mathbf{r}\,[g_{{\rm mon},cp}(r;\mu_p) - 1] = \int d\mathbf{r}\,[g_{cp,i}(r;\mu_p) - 1], \quad (3)$$

is the same for both correlation functions and directly related to the insertion free energy.[66,68] The depletion thickness is then defined as

$$\frac{4\pi}{3}\,(R_c + \delta_s)^3 = -G_{cp}, \quad (4)$$

from which it follows

$$\frac{\delta_s}{R_c} = \left(-\frac{G_{cp}}{V_c}\right)^{1/3} - 1, \quad (5)$$

where $V_c = 4\pi R_c^3/3$ is the volume of the colloid. The depletion thickness was determined for polymer systems and for single-blob models in Ref. 66. Here, we extend the calculation to the CG blob model. Results are re-

ported in Table II and summarized in Fig. 2. For $q = 0.5$ and $q = 1$, tetramer and full-monomer results are in full agreement up to $\phi_p = 2$. For $q = 2$ the tetramer slightly underestimates the depletion thickness. Nonetheless, it represents a significant improvement with respect to the single-blob model, which becomes increasingly inaccurate as ϕ_p increases. Again, this is not surprising as we expect the single-blob model to be reliable only for $q \lesssim 1$.

V. THERMODYNAMIC PROPERTIES IN THE HOMOGENEOUS PHASE

To quantify the accuracy of the CG procedure, we wish now to compare the predictions of the tetramer model with results obtained in full-monomer simulations for finite volume fractions ϕ_c and ϕ_p. This is not an easy task. Indeed, since the target functions used to determine the CG potentials were computed in the scaling limit $L \to \infty$, the tetramer model provides results that can be considered asymptotic. Therefore, a meaningful comparison requires also an extrapolation of the full-monomer results to the scaling limit, which is too demanding from the computational point of view. To avoid any extrapolation we have decided to take a slightly different approach. Instead of considering a CG tetramer model that reproduces the scaling behavior of the polymer system, we consider a CG model that is appropriate to describe Domb-Joyce chains with $L = 600$ monomers, which are taken as reference system. Then, it makes sense to compare CG results with full-monomer simulations of $L = 600$ chains at finite density, without performing any extrapolation. Of course, the price to be paid is that we need to recompute all CG potentials taking the distribution functions computed with $L = 600$ chains as targets. In the pure polymer case, results for $L = 600$ are essentially already in the scaling limit, hence there is no need to recompute the intramolecular tetramer potentials and the blob-blob intermolecular potentials. Differences of the order of a few percent are instead observed for the blob-colloid distribution functions. We have therefore recomputed the corresponding potentials. A comparison of $L = 600$ and scaling data is presented in the supplementary material:[61] differences are small, but not negligible.

In order to compare the thermodynamic behavior, we focus on the zero-momentum limit of the partial structure factors $S_{\alpha\beta,0}$ (Kirkwood-Buff integrals), which can be related to several thermodynamic quantities.[71,72] They are computed as discussed in App. A. In Table III we report their estimates for several values of ϕ_c and ϕ_p, which are close to the binodal, as predicted by GFVT.

In general, we find that the estimates of the partial structure factors $|S_{\alpha\beta,0}|$ (see App. A for definitions) increase with the number n of blobs towards the corresponding full-monomer value: $|S_{\alpha\beta,0}(n = 1)| < |S_{\alpha\beta,0}(n = 4)| \lesssim |S_{\alpha\beta,0}(\mathrm{FM})|$. The single-blob model always underestimates $|S_{\alpha\beta,0}|$: the relative difference with the full-monomer estimates increases somewhat with ϕ_c and especially with q. For $q = 2$ the model is clearly unreliable. For $q = 1$, the tetramer model gives results that are consistent with the full-monomer ones within errors, representing a significant improvement with respect to the single-blob model. For $q = 2$, tetramer results are also close to the full-monomer ones for $\phi_c = 0.1$. However, for $\phi_c = 0.2$ and 0.3, the zero-momentum structure factors are sligthly underestimated, confirming that a higher-resolution model is needed to correctly model polymer-colloid mixtures for $q = 2$.

In Table III we also report GFVT results. Since they are obtained by using scaling-limit expressions for the depletion thickness,[20,66] a small correction should be applied to the GFVT results, before comparing them with the CG and FM ones, appropriate for $L = 600$ Domb-

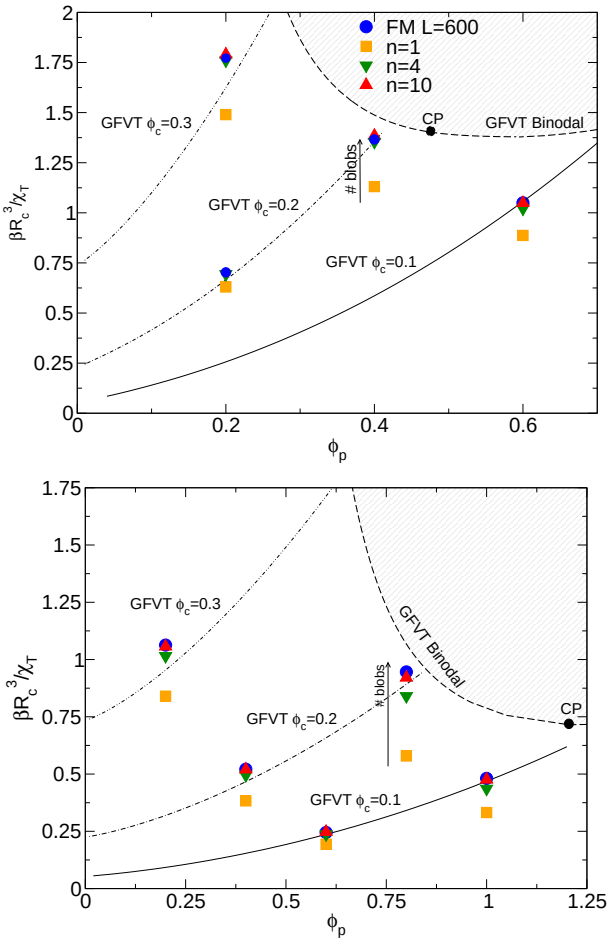

FIG. 3: Inverse isothermal compressibility as a function of ϕ_p for three values of ϕ_c, 0.1, 0.2, and 0.3. Lines give the GFVT prediction, points are simulation results obtained by using DJ L=600 chains (FM) and the corresponding CG models with $n = 1$, 4 and 10 blobs. We also report (dashed line in the upper right part of each figure) the GFVT binodal (note that in the GFVT approximation χ_T is not singular at the critical point) and the corresponding critical points (CP). Top panel refers to $q = 1$, bottom panel to $q = 2$.

TABLE III: Partial structure factors $S_{pp,0}$, $S_{cp,0}$, and $S_{cc,0}$ in the zero-momentum limit (see App. A for the definitions) for a few values of $\phi_c = 4\pi R_c^3 \rho_c/3$ and $\phi_p = 4\pi \hat{R}_g^3 \rho_p/3$. We report full-monomer (FM) and GFVT results and estimates for the CG models with $n = 1$, 4, and 10 blobs. All estimates, except the GFVT results, are appropriate for $L = 600$ Domb-Joyce chains, as explained in the text.

	q	ϕ_c	ϕ_p	FM	GFVT	$n = 1$	$n = 4$	$n = 10$
$S_{pp,0}$	1	0.1	0.6	1.46(4)	2.35	1.25(2)	1.39(4)	1.41(4)
		0.2	0.4	2.68(7)	12.2	2.00(3)	2.62(5)	2.63(3)
		0.3	0.2	2.37(9)	1.72	1.69(3)	2.25(5)	2.47(5)
	2	0.1	1.0	0.71(4)	1.47	0.522(2)	0.706(20)	0.71(2)
		0.2	0.8	2.6(3)	1.43	0.701(8)	1.55(9)	2.6(1)
		0.3	0.2	1.5(1)	0.48	0.863(4)	1.38(4)	1.58(3)
$S_{cp,0}$	1	0.1	0.6	−1.20(4)	−2.03	−1.00(2)	−1.13(4)	−1.16(4)
		0.2	0.4	−1.49(4)	−7.56	−1.07(2)	−1.46(30)	−1.48(2)
		0.3	0.2	−0.83(3)	−0.65	−0.534(1)	−0.785(20)	−0.87(2)
	2	0.1	1.0	−0.84(5)	−2.00	−0.516(4)	−0.796(25)	−0.83(2)
		0.2	0.8	−2.2(3)	−1.33	−0.472(8)	−1.25(8)	−2.2(1)
		0.3	0.2	−0.60(4)	−0.147	−0.197(1)	−0.50(2)	−0.62(1)
$S_{cc,0}$	1	0.1	0.6	1.22(4)	1.985	1.06(2)	1.15(4)	1.19(4)
		0.2	0.4	0.95(2)	4.80	0.70(1)	0.92(2)	0.94(1)
		0.3	0.2	0.36(1)	0.32	0.247(4)	0.341(8)	0.375(8)
	2	0.1	1.0	1.28(6)	3.07	0.895(6)	1.207(35)	1.27(3)
		0.2	0.8	2.0(2)	1.39	0.510(9)	1.15(7)	2.0(1)
		0.3	0.2	0.319(15)	0.136	0.143(2)	0.263(7)	0.326(5)

Joyce chains. Such correction, however, is of the order of a few percent, hence small compared with the differences we observe. For $q = 1$ and $\phi_c = 0.1$, 0.2, GFVT significantly overestimates the structure factors. This is particularly evident for $\phi_c = 0.2$, $\phi_p = 0.4$, which is very close to the GFVT critical point $\phi_{c,\mathrm{crit}} \approx 0.18$, $\phi_{p,\mathrm{crit}} \approx 0.47$, but which is far from the full-monomer critical point[20,23] $\phi_{c,\mathrm{crit}} \approx 0.22$, $\phi_{p,\mathrm{crit}} \approx 0.62$. For $q = 2$, $|S_{\alpha\beta,0}|$ is overestimated for $\phi_c = 0.1$, while it is underestimated by a factor of 2-3 for $\phi_c = 0.2$ and 0.3. The large value for $\phi_c = 0.1$ is a direct consequence of the nearby presence of the critical point (GFVT predicts $\phi_{c,\mathrm{crit}} \approx 0.11$, $\phi_{p,\mathrm{crit}} \approx 1.21$), not confirmed by the full-monomer data, that are instead consistent with the estimate[20,23] $\phi_{c,\mathrm{crit}} \approx 0.19$, $\phi_{p,\mathrm{crit}} \approx 1.08$.

As an additional check, we have computed several thermodynamic quantities that can be obtained starting from the zero-momentum partial structure factors, see appendix A for definitions and the supplementary material for an extensive list of results. In Fig. 3 we report $\beta R_c^3/\chi_T$, where χ_T is the isothermal compressibility. For both $q = 1$ and $q = 2$ single-blob results are clearly unreliable, discrepancies increasing with q and ϕ_p. Tetramer results represents a significant improvement. They fall on top of the full-monomer estimates for $q = 1$, while for $q = 2$ small differences can still be seen for $\phi_c = 0.2$ and $\phi_c = 0.3$. GFVT appears quite reliable for this quantity: unexpectedly, the discrepancies observed for $S_{\alpha\beta,0}$ cancel out in this combination. However, significant discrepancies are expected at the critical point. Indeed, at the critical point χ_T diverges. Instead, in the GFVT

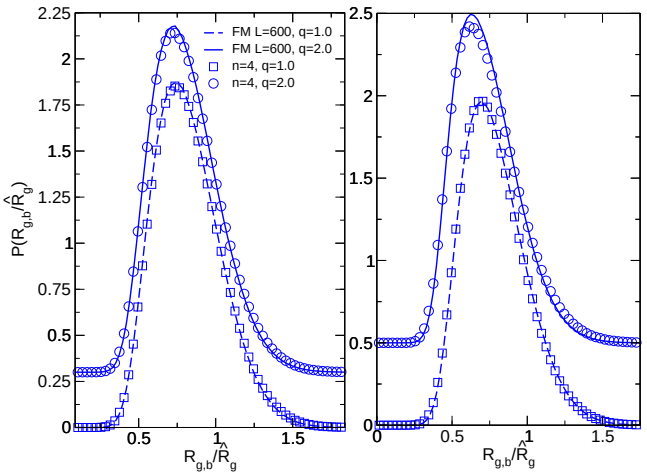

FIG. 4: Distribution functions of the radius of gyration R_{gb} of the CGR of the polymers for the tetramer. We report data for $\phi_c = 0.1$, $\phi_p = 0.6$ (left) and $\phi_c = 0.3$, $\phi_p = 0.2$ (right). The data for $q = 2$ are shifted upward by 0.3 (left) and 0.5 (right) for clarity. If we average $R_{g,b}^2$ over the distribution, we obtain $\langle R_{g,b}^2 \rangle^{1/2}/\hat{R}_g \approx 0.85$ ($q = 1$, $\phi_c = 0.1$, $\phi_p = 0.6$), 0.81 ($q = 1$, $\phi_c = 0.3$, $\phi_p = 0.2$), 0.83 ($q = 2$, $\phi_c = 0.1$, $\phi_p = 0.6$), and 0.76 ($q = 2$, $\phi_c = 0.3$, $\phi_p = 0.2$).

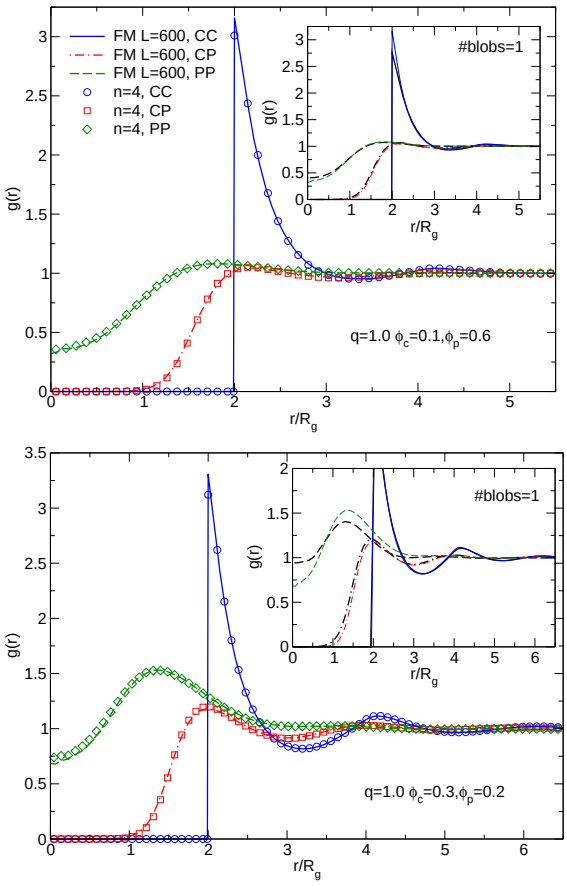

FIG. 5: Pair distribution functions between the centers of mass of the molecules as a function of $r/\hat{R}_g$: g_{cc}, g_{cp}, and g_{pp} are the colloid-colloid, colloid-polymer, and polymer-polymer functions, respectively. We report full-monomer (FM) $L = 600$ Domb-Joyce estimates and the corresponding $n = 1$ (inset), and $n = 4$ results for $q = 1$. We report results for $\phi_c = 0.1$, $\phi_p = 0.6$ (top), and for $\phi_c = 0.3$, $\phi_p = 0.2$ (bottom).

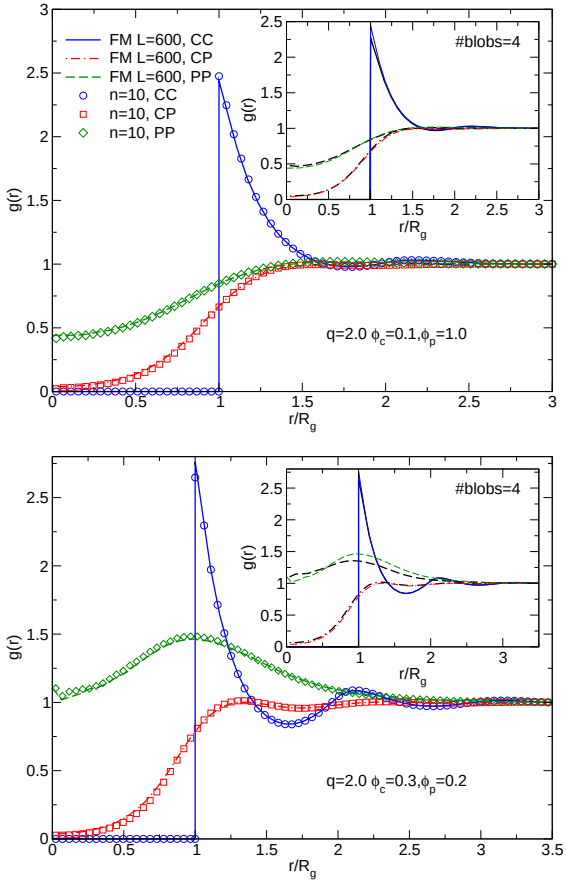

FIG. 6: Pair distribution functions between the centers of mass of the molecules as a function of $r/\hat{R}_g$: g_{cc}, g_{cp}, and g_{pp} are the colloid-colloid, colloid-polymer, and polymer-polymer functions, respectively. We report full-monomer (FM) $L = 600$ Domb-Joyce estimates and the corresponding $n = 4$ (inset) and $n = 10$ results for $q = 2$. We report results for $\phi_c = 0.1$, $\phi_p = 1.0$ (top) and for $\phi_c = 0.3$, $\phi_p = 0.2$ (bottom).

approximation χ_T is finite at criticality (GFVT is essentially a mean-field theory). Thus, it is not surprising that this approximation is not accurate for the critical point position.[20]

Let us now consider the intramolecular polymer structure. We have verified that the tetramer model reproduces well the blob-blob pair distribution function computed by using the CGR of the polymer system. As an additional check, we consider the radius of gyration of the CGR of the polymers, defined as

$$R^2_{g,b} = \frac{1}{2n^2}\sum_{i=1}^{n}(\mathbf{s}_i - \mathbf{s}_j)^2. \qquad (6)$$

Its distribution for $n = 4$ is compared with that of the radius of gyration of the tetramers in Fig. 4. The agreement is excellent, confirming the accuracy of the tetramer representation. Note also that polymers become more compact as q and/or ϕ_c increases: the distributions indeed move to the left as these two quantities become larger (additional comments and data are reported in App. B).

Finally, we consider the intermolecular structure, comparing the center-of-mass distribution functions. Results are reported in Figs. 5 and 6. For $q = 1$, the tetramer model reproduces quite well the full-monomer results. For $q = 2$, $g_{cc}(b, q)$ and $g_{cp}(b, q)$ are well reproduced. On the other hand, significant differences are observed for the polymer-polymer pair distribution function for $\phi_c = 0.3$, $\phi_p = 0.2$. This behavior is quite general: For all CG systems discrepancies always increase as ϕ_c is increased. This is not surprising, since the role of the neglected many-body colloid-polymer interactions increases as the colloid density gets larger.

VI. HIGHER-RESOLUTION MODELS AND TRANSFERABILITY

The results presented in Sec. V, show that the CG model becomes inaccurate along the binodal when the blob size is comparable with the colloid radius. Indeed, for the single-blob model, differences are observed for $q = 1$, i.e. when $\hat{R}_g$, which is the size of the blob, is equal to R_c. The tetramer begins to break down for $q = 2$, which corresponds to $\hat{r}_g/R_c \approx 0.9$ (for $n = 4$ we have[30] $\hat{r}_g/\hat{R}_g \approx 0.44$, where $\hat{r}_g$ is the blob zero-density radius of gyration). Again, blob size and colloid radius are comparable. Therefore, in order to study polymer-colloid systems in the protein regime $q > 1$, we need to develop higher-resolution models with a larger number of blobs per chain. Since[30] $\hat{r}_g/\hat{R}_g \approx n^{-\nu}$, studies of mixtures with size ratio q require CG systems with at least $n = q^{1/\nu}$ blobs.

To derive n blob models, one could address the problem directly, measuring the intermolecular blob-colloid correlation functions for a CGR of the polymer with n blobs and determine the corresponding $n/2$ potentials by using the IBI method. This is probably feasible for n not too large. Here, however, we will use a simpler approach based on the idea of the transferability of the interactions, which has been shown to work nicely for pure polymer systems, both under good-solvent conditions[31] and in the thermal crossover region.[58] Such an approach is based on the assumption that the potentials are independent of the model resolution once the blob radius of gyration $\hat{r}_g$ is used as reference length scale. In the presence of the colloids, we should also take into account a second length scale, the colloid radius R_c. If only pair interactions are relevant, it is natural to assume that the blob-colloid interactions depend only on the ratio $q_b = \hat{r}_g/R_c$ between the radius of gyration of the blob and R_c: the colloid-blob interaction is the same for systems with different resolutions but with the same q_b. If this assumption holds, we can transfer the tetramer potentials to higher-resolution CG systems. The two assumptions are essentially based on the idea that polymers are self-similar objects, so that each subchain has the same structure as the full polymer in the scaling limit.

In practice, let us indicate with $V_{cp,i}(b, q)$ the blob-colloid potential for the tetramer; here, i labels the blob along the chain and $b = r/\hat{R}_g$, where $\hat{R}_g$ is the zero-density polymer radius of gyration. Assuming transferability, we set for the potentials for the n-blob model [model (a)]:

$$V_{cp,1}(b, q; n) = V_{cp,n}(b, q; n) = V_{cp,1}(\lambda_n b, q/\lambda_n) \quad (7)$$
$$V_{cp,i}(b, q; n) = V_{cp,2}(\lambda_n b, q/\lambda_n) \qquad 2 \le i \le n-1.$$

Here λ_n is given by

$$\lambda_n = \frac{\hat{r}_g(4)}{\hat{r}_g(n)}, \quad (8)$$

where $\hat{r}_g(n)$ is the average radius of gyration of the blob in the n-blob CGR of the polymer (numerical results are reported in App. A of Ref. 30).

To verify the quality of the approximation we have considered the decamer model with $n = 10$ blobs. To derive the potentials for our reference values $q = 1$ and $q = 2$, we need to derive first the tetramer potentials for the corresponding ratios q/λ_{10}. Since[30] $\lambda_{10} = 1.702$, we have repeated the determination of the tetramer model for $q = 0.587$ and $q = 1.175$. To avoid uncertainties due to the scaling approximation we have first used the tetramer model appropriate for $L = 600$ Domb-Joyce walks.

As a first test of the decamer model, we determined the virial combinations $A_{2,cp}$, $A_{3,ccp}$, and $A_{3,cpp}$. Results, labelled (a), are reported in Table IV. The model works quite well. For $q = 1$ the predicted $A_{2,cp}$, $A_{3,cpp}$, and $A_{3,ccp}$ differ by 3%, 1%, and 3% from the full-monomer data. For $q = 2$ differences are only slightly larger (4%, 3%, 3%, respectively).

One can surmise that the small differences are end effects, which are expected to become progressively irrelevant as the number of blobs increases, related to our choice of using $V_{cp,1}(b, q)$ for the two end-blobs and $V_{cp,2}(b, q)$ for all internal blobs. To understand the sensitivity of the results on this choice, we define a second n blob model by setting [model (b)]

$$V_{cp,i}(b, q; n) = \frac{1}{2}[V_{cp,1}(\lambda_n b, q/\lambda_n) + V_{cp,2}(\lambda_n b, q/\lambda_n)], \quad (9)$$

for all i. For $n = 10$, no significant differences are observed, see Table IV, results labelled (b). Model (b) is slightly less accurate than model (a) for $q = 1$ and slightly more accurate for $q = 2$. These comparisons show that the transferability hypothesis works quite well, providing us with a model that can be used for larger values of q and ϕ_p with respect to the tetramer one.

To increase the accuracy of the CG model and obtain estimates of the virial coefficients that are as precise as the tetramer ones, we now define a third version [model (c)], in which the potentials are defined as in Eq. (9), but the length rescaling is optimized to obtained a better agreement between the full-monomer and the CG estimate of $A_{2,cp}$. We set therefore [model (c)]

$$V_{cp,i}(b, q; n) = \frac{1}{2}[V_{cp,1}(\lambda'_n b, q/\lambda_n) + V_{cp,2}(\lambda'_n b, q/\lambda_n)]. \quad (10)$$

In this expression λ_n is still given in Eq. (8), while

$$\lambda'_n = \left(\frac{A_{2,cp}(b)}{A_{2,cp}(FM)}\right)^{1/3} \frac{\hat{r}_g(4)}{\hat{r}_g(n)}, \quad (11)$$

where $A_{2,cp}(b)$ and $A_{2,cp}(FM)$ are the estimates obtained by using model (b) and the full-monomer model. If polymers were monoatomic molecules, model (c) would provide the correct estimate of $A_{2,cp}$. In our case, an exact equality does not hold. Still, model (c) reproduces the

TABLE IV: Virial combinations for full-monomer Domb-Joyce walks with $L = 600$ (FM) and for three different versions of the decamer model, as explained in the text. Symbols are the same as in Table I.

q	model	$A_{2,cp}$	$A^I_{3,cpp}$	$A^{\rm fl}_{3,cpp}$	$A_{3,cpp}$	$A^I_{3,ccp}$	$A^{\rm fl}_{3,ccp}$	$A_{3,ccp}$
1	FM	26.77(1)	134.7(2)	−5.8(1)	128.9(2)	355.2(4)	−10.8(1)	345.2(4)
	(a)	26.014(7)	134.3(3)	−6.0(2)	127.04(7)	347.1(6)	−11.4(4)	335.7(6)
	(b)	27.386(7)	141.7(3)	−6.0(2)	135.8(4)	369.2(6)	−11.4(4)	357.8(6)
	(c)	26.920(7)	138.5(3)	−6.0(2)	132.4(4)	360.6(6)	−11.0(4)	349.6(6)
2	FM	8.234(5)	26.13(3)	−1.67(2)	24.45(5)	16.60(2)	−0.87(1)	15.73(2)
	(a)	7.882(3)	25.2(1)	−1.6(1)	23.6(1)	16.14(8)	−0.88(4)	15.26(9)
	(b)	8.355(3)	26.9(1)	−1.7(1)	25.2(1)	17.00(8)	−0.92(4)	16.08(9)
	(c)	8.298(3)	26.7(1)	−1.6(1)	25.0(1)	16.85(9)	−0.91(4)	15.94(9)

full-monomer value of $A_{2,cp}$ with an error of less than 1%, which is enough for our purposes. Therefore, in the following we will consider model (c) for the decamer.

The analysis reported above was performed using the potentials appropriate for Domb-Joyce chains with $L = 600$ monomers. We have repeated the calculation determining the decamer potentials appropriate to describe polymers in the scaling limit. The corresponding virial combinations are reported in Table I. We have also recomputed the depletion thickness, see Table II and Fig. 2. The decamer and the tetramer give consistent results for both $q = 1$ and $q = 2$, indicating that both CG models describe accurately the solvation properties of a single colloid up to $\phi_p = 2$.

In the homogeneous phase close to the fluid-fluid binodal, the tetramer model is only accurate for $q = 1$. For $q = 2$ differences are clearly observed for $\phi_c = 0.2$ (close to the critical point) and for $\phi_c = 0.3$, close to the colloid-liquid phase, see Table III. For these values of ϕ_c, the tetramer model underestimates $|S_{\alpha\beta,0}|$. On the other hand, the decamer estimates are consistent with the full-monomer ones. Thus, while we expect the tetramer to provide the correct phase behavior for polymer-colloid mixtures up to $q = 1$, for $q = 2$ the decamer should be the model of choice.

We have also verified that the decamer model reproduces the intramolecular and intermolecular structure. In Fig. 7 we show the intramolecular pair distribution function $g_{\rm intra}(b)$ for the decamer. It is completely consistent with the blob-blob pair distribution function for the CGR of the polymers. A similar excellent agreement is observed for the $R_{g,b}$ distribution (not shown), confirming the good accuracy of the transferability assumption. Good agreement is also observed for the intermolecular structure, see Figs. 5 and 6. In particular, the decamer reproduces the polymer-polymer distribution function $g_{pp}(b, q)$ for $q = 2$, $\phi_c = 0.3$, $\phi_p = 0.2$, at variance with the tetramer case.

VII. THE DENSITY-DEPENDENT SINGLE-BLOB MODEL

As we have discussed, the single-blob model gives a poor description of polymer-colloid mixtures for $q \gtrsim 1$, the discrepancies increasing as the binodal is approached, see Fig. 3. Moreover, even for polymers, this CG model is not accurate as soon as $\phi_p \gtrsim 1$. We wish now to consider a variant of the single-blob model, proposed in Refs. 26,27,37,40, which considers interactions dependent on the polymer density.

For pure polymer systems the method works as follows. One considers a thermodynamic state point characterized by a volume fraction ϕ_p or, equivalently, by the excess chemical potential $\mu_p^{(\rm exc)}$ and determines the center-of-mass distribution function $g_{pp,FM}(b)$ in the polymer (full-monomer) system, where $b = r/\hat{R}_g$. Because of the equivalence of the ensembles, canonical calculations at ϕ_p and grand-canonical computations at $\mu_p^{(\rm exc)}$ give the the same result for the distribution function in the infinite-volume limit. Then, in the spirit of the structural approach, one determines the potential for the single-blob model so that the distribution function computed in the CG model is the same as the full-monomer counterpart $g_{pp,FM}(b)$. However, as discussed in Ref. 46, this second step is not defined unambiguously, as the result of the procedure depends on the ensemble. For instance, one can require the CG model to reproduce $g_{pp,FM}(b)$ in the canonical ensemble at volume fraction ϕ_p. This procedure provides a potential $V_{pp,\rm can}(b; \phi_p)$. Alternatively, one can require the CG model to reproduce $g_{pp,FM}(b)$ in the grand-canonical ensemble at $\mu_p^{(\rm exc)}$. One obtains a pair potential $V_{pp,GC}(b; \mu_p^{(\rm exc)})$, which, however, differs from the canonical one.[46] This is an intrinsic property of any structural procedure (force-matching methods do not have this limitation[46]) that maps the original system onto a CG system with state-dependent interactions.[46,48]

The above strategy can be directly extended to the mixture. Consider now a thermodynamic state point

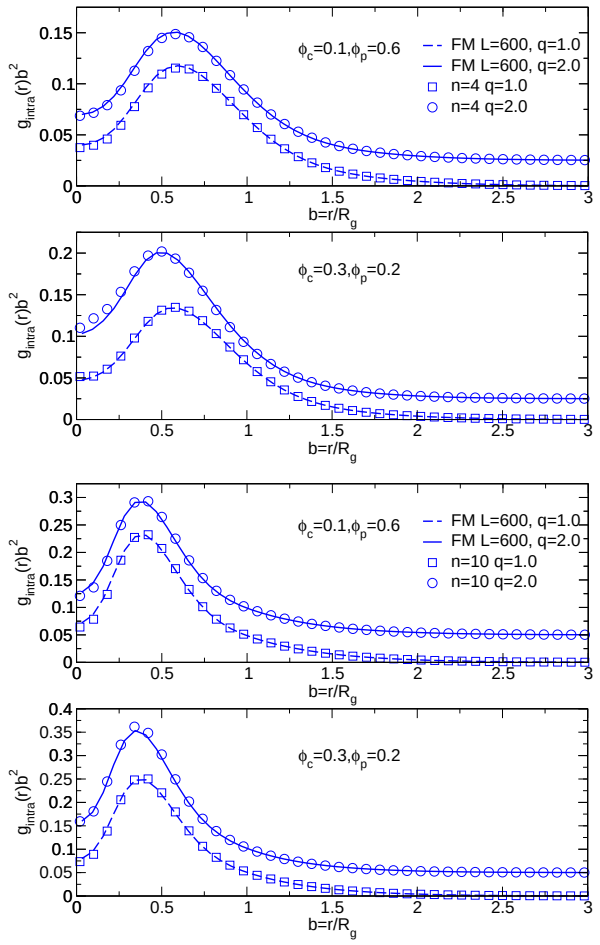

FIG. 7: Intramolecular blob-blob distribution function for $n = 4$ (two upper panels), and $n = 10$ (two lower panels) at two different state points. We report results for $q = 1$ (dashed line and squares) and $q = 2$ (continuous line and circles) versus $b = r/\hat{R}_g$. We report full-monomer CGR data (FM, lines) and results for the CG models (points). Data for $q = 2$ have been shifted upward by 0.025 for clarity.

with volume fractions ϕ_c, ϕ_p and excess chemical potentials $\mu_c^{(\rm exc)}$, $\mu_p^{(\rm exc)}$. One can compute the center-of-mass distribution functions $g_{\alpha\beta,FM}(b)$ in the full-monomer system (here α and β are indices that may refer to the polymers and to the colloids) and then determine the CG potentials by requiring the CG model to reproduce the functions $g_{\alpha\beta,FM}(b)$. As before, the result depends on the ensemble one considers, hence one obtains a different set of potentials for the canonical $[V_{\alpha\beta,\rm can}(b;\phi_c,\phi_p)]$, the semigrand-canonical $[V_{\alpha\beta,SG}(b;\phi_c,\mu_p^{(\rm exc)})]$, and the grand-canonical ensemble $[V_{\alpha\beta,GC}(b;\mu_c^{(\rm exc)},\mu_p^{(\rm exc)})]$.

A determination of the state-dependent potentials as a function of the volume fractions or of the chemical potentials is equivalent to a complete determination of the thermodynamics of the system, so that the use of state-dependent interactions would have little predictive power. Ref. 40 suggested to consider potentials parametrized by a single variable, the polymer volume fraction $\phi_p^{(r)}$ of a polymer reservoir in osmotic equilibrium with the mixture. Their approach works as follows. In the semigrand canonical ensemble, each state point is characterized by the polymer excess chemical potential $\mu_p^{(\rm exc)}$ and by the colloid volume fraction ϕ_c. Instead of using $\mu_p^{(\rm exc)}$, one can equivalently (but note that the equivalence only holds in the original, full-monomer system) consider the polymer volume fraction $\phi_p^{(r)}$. If an accurate expression of the polymer equation of state is available, $\phi_p^{(r)}$ can be determined by inverting the relation

$$\beta\mu_p^{(exc)} = \int_0^{\phi_p} \frac{d\sigma}{\sigma}(K_p(\sigma,0)-1), \qquad (12)$$

where

$$K_p(\phi_p,\phi_c) = \left(\frac{\partial\beta P}{\partial\rho_p}\right)_{\rho_c}. \qquad (13)$$

Then, the potentials of the CG model at ϕ_c and $\mu_p^{(\rm exc)}$ is defined as[73]

$$V_{\alpha\beta,SG}(b;\phi_c,\mu_p^{(\rm exc)}) = V_{\alpha\beta,\rm can}(b;0,\phi_p^{(r)}), \qquad (14)$$

where the right-hand side is computed at zero colloidal density. In practice, $V_{cc,\rm can}(b;0,\phi_p^{(r)})$ is the usual hard-core pair potential, while $V_{pp,\rm can}(b;0,\phi_p^{(r)})$ is the canonical potential defined before in the case of the single-component polymer system. The colloid-polymer potential $V_{cp,\rm can}(b;0,\phi_p^{(r)})$ is also determined in the canonical ensemble at $\phi_p^{(r)}$. One determines the polymer density profile $g_{cp,FM}(b)$ around a colloid as a function of b and then fixes the potential by requiring the CG model to reproduce $g_{cp,FM}(b)$ in the *canonical ensemble*.

Choice (14) is by no means unique and indeed, a conceptually equivalent approximation in the semigrand-canonical ensemble is (model SB-SG)

$$V_{\alpha\beta,SG}(b;\phi_c,\mu_p^{(\rm exc)}) = V_{\alpha\beta,SG}(b;0,\mu_p^{(\rm exc)}), \qquad (15)$$

where the right-hand side is computed at zero colloidal density. The potentials in the right-hand side are obtained by considering the same target functions $g_{pp,FM}(b)$ and $g_{cp,FM}(b)$ as before, but now the equality of the structural properties is obtained in the polymer grand-canonical ensemble at zero colloidal density.

If one is only interested in properties of the homogeneous phase, one might consider the mixture in the canonical ensemble. Again, the choice of the potential set is ambiguous. Here we consider two possibilities. First, we define (model SB-can)

$$V_{\alpha\beta,\rm can}(b;\phi_c,\phi_p) = V_{\alpha\beta,\rm can}(b;0,\phi_p^{(r)}), \qquad (16)$$

where the reservoir polymer volume fraction $\phi_p^{(r)}$ is defined before. Another possibility is simply (model SB-ϕ_p)

$$V_{\alpha\beta,\rm can}(b;\phi_c,\phi_p) = V_{\alpha\beta,\rm can}(b;0,\phi_p). \qquad (17)$$

As a case study, we first consider a polymer-colloid mixture with $q = 1$, the value of q where the zero-density single-blob model begins to break down. We take $\phi_c = 0.2$, $\phi_p = 0.2$, and, as in Sec. V, we take the Domb-Joyce model with $L = 600$ as reference system. At this state point the tetramer model reproduces correctly the structure and the thermodynamics of the mixture (see supplementary material[61]) and can be used to obtain some quantities hardly measurable with full-monomer simulations of long polymers. One such quantity is the polymer chemical potential, which can be determined by using Widom's insertion method. In the tetramer model we obtain $\beta\hat{\mu}_p = 1.15356$, where

$$\beta\hat{\mu}_p = \log\phi_p + \beta\mu_p^{(exc)}. \qquad (18)$$

The quantity $\hat{\mu}_p$ differs from μ_p by a density-independent constant that depends on the detailed intramolecular structure, but it has the advantage that, at a given state point, it is the same in the full-monomer model and in the CG ones. Using the accurate equation of state of Ref. 74 and Eq. (12), we obtain $\phi_p^{(r)} = 0.565$. Once $\phi_p^{(r)}$ and $\beta\hat{\mu}_p$ for the reservoir are known, we should compute the CG potentials. Instead of performing a direct numerical inversion, using the iterative Boltzmann inversion method for instance, one can use integral-equation methods.[26,27,38,45] For both ensembles, we use the hypernetted-chain (HNC) approximation which turns out to be quite accurate (see App. C for a discussion of the grand-canonical case). Once the potentials have been obtained, we have verified their accuracy. For each model, we have performed Monte Carlo simulations in the appropriate ensemble, computing the distribution functions and comparing the results with the full-monomer estimates. As an example, in Fig. 8 we show the results obtained in canonical-ensemble simulations of the model with potentials (16). Comparison with the full-monomer target functions shows that the inversion procedure is quite accurate. The quality of the inversion can also be tested by computing some thermodynamic observables that are related to the target structural quantities through simple sum rules, and that are strongly influenced by the accuracy of the tails of the potentials. For instance, we have computed the pressure derivative K_p, Eq. (13). In the canonical ensemble at $\phi_p^{(r)} = 0.565$ we obtain $K_p = 2.95(5)$ for model (SB-can), which is in good agreement with the full-monomer estimate $K_p = 2.94$, obtained by using the equation of state of Ref. 74. Analogously, we compute the polymer depletion thickness, finding $\delta_s/R_c = 0.55(1)$ to be compared with the full-monomer result 0.53(3). It is also interesting to compute the same quantities in the tetramer model: we have $K_p = 2.90(4)$ and 0.54(1), respectively, again in good agreement with the full-monomer predictions. Note that our potentials differ from those reported in Ref. 45, since here we consider polymers in the scaling limit, while the potentials of Ref. 45 are appropriate for self-avoiding walks with 500 monomers.

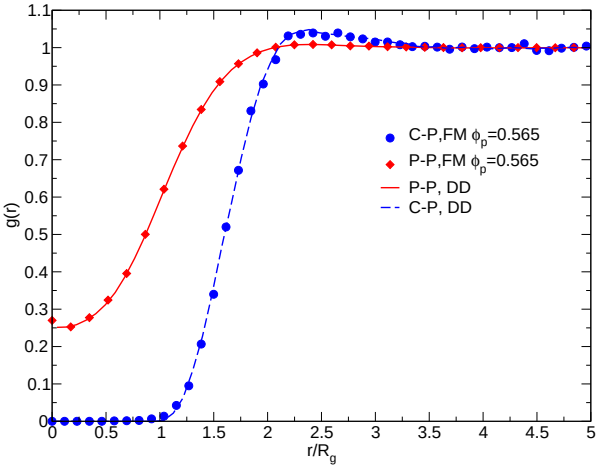

FIG. 8: Polymer-polymer and polymer-colloid distribution functions (for the polymers we consider its center of mass). We report full-monomer data and canonical-ensemble simulation results for the density-dependent (DD) single-blob (SB-can) model with potentials (16) at $\phi_p = 0.565$ and zero colloidal density. Here $q = 1$.

The nonequivalence of the two ensembles for density-dependent models implies that not all quantities are reproduced by the CG model, even at $\phi_c = 0$.[46] For instance, let us consider the pure polymer model in the canonical ensemble at $\phi_p^{(r)} = 0.565$ and let us compute the chemical potential by Widom's method. The CG model gives $\beta\hat{\mu}_p = 1.2530(2)$, which is different from the the value of the chemical potential at the reference point. Viceversa, if we consider the grand-canonical ensemble at $\hat{\mu}_p = 1.15356$ we obtain a volume fraction $\phi_p^{(r)} = 0.546$, which differs by 3.5% from the reference value.

Once we have determined the density-dependent potentials, we can use them to compute thermodynamic properties of the mixture. First, we compare two different choices of potentials that look most natural: a) we perform semigrand-canonical simulations at $\hat{\mu}_p = 1.15356$ and $\phi_c = 0.2$ using the CG model with potentials (15); b) we perform canonical simulations at $\phi_p = 0.2$ and $\phi_c = 0.2$ using the CG model with potentials (16). We compare the results of these simulations with canonical full-monomer and zero-density single-blob estimates. Results are reported in Table V. For the zero-momentum structure factors, the estimates obtained in state-dependent models are significantly worse than the results of the zero-density single-blob model. Also the second-order derivative of the Gibbs free energy g'' (see App. A) is determined more accurately by the standard single-blob model than by the state-dependent ones.

TABLE V: Comparison of single-blob results for state point $q = 1, \phi_c = 0.2, \phi_p = 0.2$. We report canonical results for the full-monomer (FM) model, the zero-density single-blob (SB) model, the canonical density-dependent single-blob (SB-can) model [potentials (16)], and the density-dependent single-blob (SB-ϕ_p) model at fixed ϕ_p [potentials (17)]. Results labelled SB-SG are obtained in semigrand-canonical simulations using potentials (15). The input quantities are reported in boldface. The FM value for $\beta\hat{\mu}_p$ (in brackets) has been determined by using the tetramer model. See App. A for the definitions of the thermodynamic quantities.

	FM	SB	SB-can	SB-SG	SB-ϕ_p
$\beta\hat{\mu}_p$	[1.15356]	0.9970(6)	1.2898(4)	**1.15356**	1.0784(3)
ϕ_p	**0.2**	**0.2**	**0.2**	0.18360(3)	**0.2**
$S_{pp,0}$	1.48(10)	1.44(1)	1.86(2)	1.85(2)	1.51(1)
$S_{cp,0}$	−0.66(5)	−0.619(8)	−0.86(1)	−0.85(1)	−0.658(9)
$S_{cc,0}$	0.44(2)	0.428(5)	0.562(7)	0.553(8)	0.449(5)
K_p	5.01(6)	4.42(3)	4.76(1)	4.70(1)	4.54(1)
K_c	9.72(5)	8.73(6)	9.09(4)	8.72(4)	8.88(3)
$\frac{\beta R_c^3}{\chi_T}$	0.703(5)	0.63(4)	0.661(2)	0.622(2)	0.641(2)
$1/g''$	0.41(3)	0.389(4)	0.518(6)	0.519(6)	0.409(4)

Since this quantity is an order parameter for the critical point, it is not clear if phase behavior is determined more accurately by using single blob models defined at zero density or by models with state-dependent interactions. On the other hand, for some other observables, like the pressure derivatives K_p and K_c, the state-dependent models give estimates that are closer to the full-monomer results than those of the single-blob model defined at zero density.

As a final remark, let us consider the canonical CG model at $\phi_p = 0.2$ and $\phi_c = 0.2$ with potentials (17). Since the polymer density at which the potentials are computed is small, results are not too different from those of the zero-density single-blob model. Discrepancies with the full-monomer result are however smaller. Note, however, that this approach cannot be used to investigate phase separation, since the coexisting phases would be associated with different pair potentials. This is not the case of potentials (14) and (15), which could both be employed to estimate the fluid-fluid binodals.

The same study has been performed for $q = 0.5$ at the thermodynamic state $\phi_c = 0.2, \phi_p = 0.1$, at which the tetramer model predicts a chemical potential $\hat{\mu}_p = -1.05322$, that corresponds to a reservoir volume fraction $\phi_p^{(r)} \approx 0.2$. Since $\phi_p^{(r)}$ is small, the ensemble dependence of the potentials is tiny. Moreover, they show only small differences with respect to their zero-density counterparts. Results are compared in Table VI. For this value of q, the state-dependent results are in better agreement with full-monomer and tetramer results than the single-blob estimates, which are, however, already in reasonable agreement.

The analysis presented here shows that the use of state-dependent potentials does not provide a systematic improvement with respect to the zero-density single-blob model. Apparently, there is no clear advantage in using state-dependent potentials, instead of those defined at zero polymer density.

VIII. CONCLUSIONS

In this paper we determine a fully consistent multi-blob model for mixtures of hard-sphere colloids and linear polymers under good-solvent conditions. We use the structure-based route, determining the effective potentials at zero polymer and colloidal density. This allows us to avoid all ambiguities related to the use of state-dependent interactions.[46,48] Moreover, at zero density it is easy to compute properties in the scaling limit, which are then used as target functions to construct the CG model. As a consequence, the resulting CG models allow us to determine thermodynamic and structural properties directly in the scaling limit with a limited computation effort. Hence, no extrapolations in the polymer length are needed before comparing with the results of experiments with high molecular-weight polymers. As in our previous work,[30,31] we start by representing polymers with a tetramer chain of four blobs and parametrizing polymer-colloid interactions with blob-colloid pair potentials. We show that such a model is quite accurate in the homogeneous phase for $q \lesssim 1$. It reproduces both the intramolecular and intermolecular structure on scales $r \gtrsim \hat{r}_g$, where $\hat{r}_g$ is the zero-density blob radius of gyration. Also thermodynamics is well reproduced. For $q = 2$, we observe small differences between tetramer and full-monomer estimates, which increase with colloid and polymer densities. To investigate the behavior of the mixture for larger values of q, higher-resolution models are needed. We show that a simple transferability assumption of the blob-colloid potentials makes the model fully transferable with the number n of blobs. Indeed, the blob-colloid pair potentials for $n > 4$ can be obtained from the tetramer ones by performing simple length rescalings. The basic assumption, which is confirmed by the numerical results, is that potentials are resolution independent, if the blob radius of gyration $\hat{r}_g$ is taken as reference length scale and if the ratio $q_b = \hat{r}_g/R_c$ is assumed as reference polymer-to-colloid size ratio. We explicitly consider the decamer model with $n = 10$ blobs. We find it to be accurate for $q \lesssim 2$ in the homogeneous phase, below the demixing binodal.

We also discuss in detail single-blob models with state-dependent potentials. We consider several variants—as discussed in Ref. 46, state-dependent potentials depend both on the thermodynamic state and on the ensemble considered. If potentials are independent of the colloidal density, as is the case for the models discussed in Refs. 40,

TABLE VI: Comparison of single-blob results for state point $q = 0.5, \phi_c = 0.2, \phi_p = 0.1$. Symbols are defined as in Table V.

	FM	SB	SB-can	SB-GC	$n = 4$
$\beta\hat{\mu}_p$		$-1.0659(1)$	$-1.0483(1)$	$\mathbf{-1.0532}$	$-1.0532(1)$
ϕ_p	**0.1**	**0.1**	**0.1**	0.09956(1)	**0.1**
$S_{pp,0}$	1.86(7)	1.674(5)	1.759(5)	1.73(2)	1.713(8)
$S_{cp,0}$	$-0.62(2)$	$-0.553(3)$	$-0.591(3)$	$-0.577(9)$	$-0.572(4)$
$S_{cc,0}$	0.339(8)	0.317(2)	0.333(2)	0.325(5)	0.322(2)
K_p	2.64(2)	2.648(2)	2.671(2)	2.673(6)	2.706(4)
K_c	12.62(6)	12.41(2)	12.51(2)	12.54(2)	12.72(3)
$\frac{\beta R_c^3}{\chi_T}$	1.107(6)	1.098(1)	1.107(1)	1.107(4)	1.112(2)
$1/g''$	0.182(6)	0.1649(8)	0.1746(8)	0.172(2)	0.169(1)

41,45, the predictions of these models are significantly less accurate than those of the multiblob model.

Our model can be readily used to study the phase diagram of polymer-colloid solutions under good-solvent conditions. This study is technically difficult at the full-monomer level. Simulation studies are limited to quite short chains,[22–24] so that results are affected by large scaling corrections. As a consequence, extrapolations must be performed,[20] adding a considerable amount of uncertainty on the final results, before comparing simulation results with experimental data on high-molecular-weight polymer solutions.

Along the lines of our previous work on polymer solutions,[58] our strategy can be extended to investigate mixtures in the thermal crossover region (within the GFVT approximation, this issue has already been discussed in Ref. 20). The same strategy could also be extended to different systems with a characteristic mesoscopic length scale, for instance, to stretched chains and networks, polymers of different architecture, tethered chains, and solutions with colloids of nonspherical shape. Also in this case a multiblob approach should be quantitatively accurate, as long as the blob size is comparable or smaller than all characteristic length scales of the system. Transferability with the number of blobs should also work in general, as it is based on the self-similar structure of the polymers.

Appendix A: Structure factors and thermodynamic properties

In this appendix we collect some formulae that allow one to compute thermodynamic properties from structural estimates. For the sake of generality, let us consider a binary mixture of two types of molecules, which have L_1 and L_2 atoms each. If there are N_α molecules of type α in a volume V, the structure factor $S_{\alpha\beta}(\mathbf{k})$ is defined as

$$S_{\alpha\beta}(\mathbf{k}) = \frac{1}{L_\alpha L_\beta \sqrt{N_\alpha N_\beta}} \left\langle \sum_{ij,AB} e^{i\mathbf{k}\cdot(\mathbf{r}_{iA}^{(\alpha)} - \mathbf{r}_{jB}^{(\beta)})} \right\rangle, \quad \text{(A1)}$$

where $\mathbf{r}_{iA}^{(\alpha)}$ is the position of atom i belonging to molecule A of type α. Analogously, we define the pair correlation function

$$g_{\alpha\beta}(\mathbf{r}_1 - \mathbf{r}_2) = \frac{1}{L_\alpha L_\beta \rho_\alpha \rho_\beta} \times \left\langle {\sum_{AB}}' \sum_{ij} \delta(\mathbf{r}_1 - \mathbf{r}_{iA}^{(\alpha)}) \delta(\mathbf{r}_2 - \mathbf{r}_{jB}^{(\beta)}) \right\rangle, \quad \text{(A2)}$$

where $\rho_\alpha = N_\alpha/V$ is the density of the α molecules and the prime in the summation over A and B indicates that terms with $A = B$ should not be considered if $\alpha = \beta$. Then, it is easy to show that

$$S_{\alpha\beta}(\mathbf{k}) = \sqrt{N_\alpha N_\beta}\delta_{\mathbf{k},\mathbf{0}} + \delta_{\alpha\beta} F_\alpha(\mathbf{k}) + \sqrt{\rho_\alpha \rho_\beta} \int (g_{\alpha\beta}(\mathbf{r}) - 1) e^{i\mathbf{k}\cdot\mathbf{r}} d\mathbf{r}, \quad \text{(A3)}$$

where

$$F_\alpha(\mathbf{k}) = \frac{1}{L_\alpha^2 N_\alpha} \left\langle \sum_{ij,A} e^{i\mathbf{k}\cdot(\mathbf{r}_{iA}^{(\alpha)} - \mathbf{r}_{jA}^{(\alpha)})} \right\rangle \quad \text{(A4)}$$

is the form factor of the α molecules. If we introduce the Kirkwood-Buff integrals[71]

$$G_{\alpha\beta} = \int (g_{\alpha\beta}(\mathbf{r}) - 1) d\mathbf{r}, \quad \text{(A5)}$$

we obtain

$$S_{\alpha\beta,0} = \lim_{k\to 0} S_{\alpha\beta}(\mathbf{k}) = 1 + \sqrt{\rho_\alpha \rho_\beta} G_{\alpha\beta}. \quad \text{(A6)}$$

The quantities $S_{\alpha\beta,0}$ are related to thermodynamics by fluctuation theorems. In the grand-canonical ensemble we have[68,72]

$$\frac{1}{V}\left(\langle N_\alpha N_\beta\rangle - \langle N_\alpha\rangle\langle N_\beta\rangle\right) = \sqrt{\rho_\alpha\rho_\beta}S_{\alpha\beta,0}. \tag{A7}$$

Using this result we can express several thermodynamic quantities in terms of $S_{\alpha\beta,0}$. We define

$$|S_0| = S_{11,0}S_{22,0} - S_{12,0}^2. \tag{A8}$$

Then, the density derivatives of the pressure P in the canonical ensemble can be written as

$$K_\alpha \equiv \left(\frac{\partial\beta P}{\partial\rho_\alpha}\right)_{\rho_\beta} = |S_0|^{-1}(S_{\beta\beta,0} - \sqrt{\rho_\beta/\rho_\alpha}S_{\alpha\beta,0}). \tag{A9}$$

If we now consider the isobaric (P, N_1, N_2) ensemble and write the Gibbs free energy as $\beta G(P, N_1, N_2) = (N_1 + N_2)g(P, x_1)$, $x_1 = N_1/(N_1 + N_2)$, we obtain

$$\begin{aligned}\frac{1}{g''} &= \left(\frac{\partial^2 g}{\partial x_1^2}\right)_P^{-1} \\ &= x_1x_2\left(x_1S_{22,0} + x_2S_{11,0} - 2\sqrt{x_1x_2}S_{12,0}\right),\end{aligned} \tag{A10}$$

where $x_2 = 1 - x_1$. As for the isothermal compressibility

$$\chi_T = -\frac{1}{V}\left(\frac{\partial V}{\partial P}\right)_{N_1,N_2}, \tag{A11}$$

we obtain

$$\frac{\beta}{\chi_T} = |S_0|^{-1}(\rho_1S_{22,0} + \rho_2S_{11,0} - 2\sqrt{\rho_1\rho_2}S_{12,0}). \tag{A12}$$

In order to use these expressions, we must determine the structure factors in the limit $k \to 0$. We use here the method discussed in Refs. 66,74. We consider a cubic box of size $V = M^3$ and determine $S_{\alpha\beta}(\mathbf{k})$ for the smallest values available in a cubic box. We choose $\mathbf{k}_a = (k_a, 0, 0)$ and $k_1 = 2\pi/M$, $k_2 = 2k_1$, $k_3 = 3k_1$, $k_4 = 4k_1$. Then, we consider the approximants

$$\begin{aligned}S_{\alpha\beta}^{(1)} &= \frac{4}{3}S_{\alpha\beta}(\mathbf{k}_1) - \frac{1}{3}S_{\alpha\beta}(\mathbf{k}_2), \\ S_{\alpha\beta}^{(2)} &= \frac{3}{2}S_{\alpha\beta}(\mathbf{k}_1) - \frac{3}{5}S_{\alpha\beta}(\mathbf{k}_2) + \frac{1}{10}S_{\alpha\beta}(\mathbf{k}_3), \\ S_{\alpha\beta}^{(3)} &= \frac{8}{5}S_{\alpha\beta}(\mathbf{k}_1) - \frac{4}{5}S_{\alpha\beta}(\mathbf{k}_2) \\ &\quad + \frac{8}{35}S_{\alpha\beta}(\mathbf{k}_3) - \frac{1}{35}S_{\alpha\beta}(\mathbf{k}_4).\end{aligned} \tag{A13}$$

Since $k \approx 1/M$, it is easy to show that $S_{\alpha\beta}^{(n)} = S_{\alpha\beta,0} + O(M^{-2n-2})$. Note that we do not consider the volume corrections (of order $1/V = M^{-3}$ see, e.g., Ref. 75), which affect $S_{\alpha\beta}(\mathbf{k})$ at fixed k. For the typical volumes we consider, such corrections are negligible (see Ref. 58 for the analogous discussion concerning the polymer-polymer distribution function). For the values of ϕ_c and ϕ_p we investigate and for our typical volumes, we observe some differences between $S_{\alpha\beta}^{(1)}$ and $S_{\alpha\beta}^{(2)}$, while $S_{\alpha\beta}^{(2)} \approx S_{\alpha\beta}^{(3)}$ within errors. Hence, we take approximant $S_{\alpha\beta}^{(2)}$ as our estimate of $S_{\alpha\beta,0}$.

In the GFVT we have direct access to the thermodynamic properties. The GFVT estimates of the zero-momentum factors $S_{\alpha\beta,0}$ are obtained by using the grand-canonical relation

$$\left(\frac{\partial\rho_\alpha}{\partial\beta\mu_\beta}\right)_{GC} = \sqrt{\rho_\alpha\rho_\beta}S_{\alpha\beta,0}, \tag{A14}$$

which is a direct consequence of Eq. (A7).

Appendix B: The radius of gyration of the polymer and of the blobs

In this Appendix we discuss how the sizes of the polymers and of the blobs change in the homogeneous phase as ϕ_c and ϕ_p vary. In Table VII we report full-monomer results for $L = 600$ Domb-Joyce chains—they are not asymptotic, but we expect differences to be relatively small. Let us first consider the ratio $R_g(\phi_c, \phi_p)/\hat{R}_g$, where $\hat{R}_g$ is the zero-density radius of gyration. For $\phi_c = 0$ the ratio $R_g(0, \phi_p)/\hat{R}_g = f_g(\phi_p)$ was computed in Refs. 74,76, obtaining the interpolation formula

$$f_g(\phi_p) = \frac{(1 + 0.33272\phi_p)^{0.0575}}{(1 + 0.98663\phi_p + 0.49944\phi_p^2 + 0.049597\phi_p^3)^{0.0575}}. \tag{B1}$$

The size decreases as ϕ_p increases, but quite slowly: $f_g(\phi_p) \approx \phi_p^{-0.11}$ for large ϕ_p. For $\phi_c \neq 0$, the data show that the size of the polymers depends crucially on q and that, for the same volume fractions ϕ_c and ϕ_p, polymers become more compact as q increases. For instance, for $\phi_c = 0.3$ and $\phi_p = 0.2$, we have $R_g(\phi_c, \phi_p)/\hat{R}_g = 0.92, 0.87, 0.81$ for $q = 1, 2$ and 4, respectively. This phenomenon, which has already been noted in Ref. 77 for $\phi_p = 0$, is connected to the sharp decrease of the free-volume factor as q increases. When q gets larger at fixed ϕ_c and ϕ_p, the available space for the insertion of the polymer decreases, hence polymers become more compact.

In Table VII we also report the average radius of gyration $r_g(n)$ of the blobs for different CGRs of the polymers. The n dependence of the zero-density quantity $\hat{r}_g(n)$ was discussed in Ref. 30, where it was shown that for all $n \geq 4$ one can write

$$\frac{\hat{r}_g(n)}{\hat{R}_g} = kn^{-\nu} \qquad k = 1.03 - 0.04/n. \tag{B2}$$

Here we discuss its behavior in the homogeneous phase with the purpose of verifying one of the basic assumptions of the CG approach. The n-blob CG model is predictive

TABLE VII: Blob radius of gyration $r_g(n)$ for the CGR of the polymer in terms of n blobs and radius of gyration R_g of the polymer as a function of q, ϕ_c, and ϕ_p. All quantities are expressed in terms of the zero-density radius of gyration $\hat{R}_g$ of the polymer. The effective volume fraction $\phi_{p,\rm app}$ is defined as the volume fraction of the pure polymeric system for which one has the same value of the ratio $R_g/\hat{R}_g$, i.e. $R_g/\hat{R}_g = f_g(\phi_{p,\rm app})$, where $f_g(\phi_p)$ is defined in Eq. (B1).

q	ϕ_c	ϕ_p	$r_g(4)/\hat{R}_g$	$r_g(10)/\hat{R}_g$	$r_g(20)/\hat{R}_g$	$r_g(30)/\hat{R}_g$	$R_g/\hat{R}_g$	$\phi_{p,\rm app}$
	0.0	0.0	0.4518	0.2654	0.1771	0.1397	1	0
0.5	0.2	0.1	0.4484	0.2648	0.1773	0.1401	0.9766	0.624
1	0.1	0.6	0.4439	0.2635	0.1767	0.1398	0.9578	1.184
	0.1	0.8	0.4422	0.2629	0.1765	0.1396	0.9503	1.431
	0.1	1.0	0.4405	0.2624	0.1763	0.1395	0.9437	1.666
	0.2	0.2	0.4431	0.2634	0.1767	0.1398	0.9508	1.416
	0.2	0.4	0.4411	0.2627	0.1765	0.1396	0.9424	1.712
	0.3	0.2	0.4376	0.2618	0.1762	0.1395	0.9219	2.554
2	0.1	0.6	0.4400	0.2622	0.1762	0.1395	0.9432	1.684
	0.1	1.0	0.4367	0.2611	0.1758	0.1392	0.9301	2.198
	0.2	0.4	0.4326	0.2599	0.1754	0.1390	0.9102	3.125
	0.2	0.8	0.4291	0.2586	0.1749	0.1387	0.8974	3.837
	0.3	0.2	0.4229	0.2568	0.1742	0.1384	0.8671	6.023
4	0.3	0.2	0.4018	0.2480	0.1702	0.1360	0.8121	12.67

as long as the structure of the blobs does not play any role in the determination of the large-scale properties of the system. This implies that the CG model provides a good approximation at (ϕ_c, ϕ_p), if $r_g(\phi_c, \phi_p, n) \approx \hat{r}_g(n)$. Data shown in Table VII support this approximate equality. In all cases, differences decrease with n—the larger n is, the more accurate the CG description is—and increase as q gets larger— the accuracy of the n blob model worsens as q increases.

Appendix C: Grand-canonical single-blob models and integral equations

The state-dependent single-blob potentials can be accurately determined by using integral-equation methods.[68] Canonical-ensemble potentials (models SB-can and SB-ϕ_p) are derived as in Refs. 26,45. The grand-canonical potentials $V_{\alpha\beta,SG}(b; 0, \mu_p^{(\rm exc)})$ are determined analogously, using the HNC relation[78,79] between chemical potential and density ρ_p,

$$\mu_p^{(\rm exc)} = \frac{\rho_p}{2} \int d^3\mathbf{r} \left[h_{pp}(\mathbf{r})^2 - h_{pp}(\mathbf{r}) c_{pp}(\mathbf{r}) - 2 c_{pp}(\mathbf{r}) \right]. \tag{C1}$$

Here $h_{pp}(\mathbf{b}) = g_{pp,FM}(\mathbf{b}; \mu_p^{(\rm exc)}) - 1$ and the direct correlation function $c_{pp}(\mathbf{b})$ is defined by the Ornstein-Zernike relation[68]

$$h_{pp}(\mathbf{b}) = c_{pp}(\mathbf{b}) + \rho_p \int d^3\mathbf{s}\, c_{pp}(\mathbf{s}) h_{pp}(\mathbf{b} - \mathbf{s}). \tag{C2}$$

Solving simultaneously Eqs. (C1) and (C2) we obtain ρ_p and $c_{pp}(\mathbf{b})$. The polymer-polymer potential follows from the HNC closure relation:

$$\beta V_{pp,SG}(\mathbf{b}; \mu_p^{(\rm exc)}) = h_{pp}(\mathbf{b}) - c_{pp}(\mathbf{b}) - \ln g_{pp,FM}(\mathbf{b}; \mu_p^{(\rm exc)}). \tag{C3}$$

The polymer-colloid potential is determined as[45]

$$\beta V_{cp,SG}(\mathbf{b}; \mu_p^{(\rm exc)}) = -\log(h_{cp}(\mathbf{b}) + 1) + \rho_p \int d^3\mathbf{s}\, c_{pp}(\mathbf{s}) h_{cp}(\mathbf{b} - \mathbf{s}), \tag{C4}$$

which is obtained by using the two-component Ornstein-Zernike relation[68] in the limit $\rho_c \to 0$ and the HNC closure relation for the polymer-colloid potential. Here $h_{cp}(\mathbf{b}) = g_{cp,FM}(\mathbf{b}, \mu_p^{(exc)}) - 1$.

* Electronic address: giuseppe.dadamo@sissa.it
† Electronic address: andrea.pelissetto@roma1.infn.it
‡ Electronic address: carlo.pierleoni@aquila.infn.it

[1] W. C. K. Poon, J. Phys.: Condensed Matter **14**, R859 (2002).
[2] M. Fuchs and K. S. Schweizer, J. Phys.: Condensed Matter

14, R239 (2002).
[3] V. J. Anderson and H. N. W. Lekkerkerker, Nature **416**, 811 (2002).
[4] R. Tuinier, J. Rieger, and C. G. de Kruif, Adv. Colloid Interface Sci. **103**, 1 (2003).
[5] K. J. Mutch, J. S. van Duijneveldt, and J. Eastoe, Soft Matter **3**, 155 (2007).
[6] G. J. Fleer and R. Tuinier, Adv. Coll. Interface Sci. **143**, 1 (2008).
[7] O. Myakonkaya and J. Eastoe, Adv. Coll. Interface Sci. **149**, 39 (2009).
[8] M. Fuchs and K. S. Schweizer, Europhys. Lett. **51**, 621 (2000).
[9] M. Fuchs and K. S. Schweizer, Phys. Rev. E **64**, 021514 (2001).
[10] S. Ramakrishnan, M. Fuchs, K. S. Schweitzer, and C. F. Zukoski, J. Chem. Phys. **116**, 2201 (2002).
[11] M. Schmidt, A. R. Denton, and J. M. Brader, J. Chem. Phys. **118**, 1541 (2003).
[12] P. Bryk, J. Chem. Phys. **122**, 064902 (2005).
[13] P. Paricaud, S. Varga, and G. Jackson, J. Chem. Phys. **118**, 8525 (2003).
[14] A. Pelissetto and J. P. Hansen, Macromolecules **39**, 9571 (2006).
[15] H. N. W. Lekkerkerker, W. C. K. Poon, P. N. Pusey, A. Stroobants, and P. B. Warren, Europhys. Lett. **20**, 559 (1992).
[16] D. G. L. Aarts, R. Tuinier, and H. N. W. Lekkerkerker, J. Phys.: Condens. Matt. **14**, 7551 (2002).
[17] G. J. Fleer and R. Tuinier, Phys. Rev. E **76**, 041802 (2007).
[18] R. Tuinier, P. A. Smith, W. C. K. Poon, S. U. Egelhaaf, D. G. A. L. Aarts, H. N. W. Lekkerkerker, and G. J. Fleer, Europhys. Lett. **82**, 68002 (2008).
[19] H. N. W. Lekkerkerker and R. Tuinier, *Colloids and the Depletion Interaction*, Lect. Notes Phys. **833** (Springer, Berlin, 2011).
[20] G. D'Adamo, A. Pelissetto, and C. Pierleoni, J. Chem. Phys. **141**, 024902 (2014).
[21] P. G. Bolhuis, E. J. Meijer, and A. A. Louis, Phys. Rev. Lett. **90**, 068304 (2003).
[22] C.-Y. Chou, T. T. M. Vo, A. Z. Panagiotopoulos, and M. Robert, Physica A **369**, 275 (2006).
[23] N. A. Mahynski, T. Lafitte, and A. Z. Panagiotopoulos, Phys. Rev. E **85**, 051402 (2012).
[24] N. A. Mahynski, B. Irick, and A. Z. Panagiotopoulos, Phys. Rev. E **87**, 022309 (2013).
[25] C. N. Likos, Phys. Rep. **348**, 267 (2001).
[26] A. A. Louis, P. G. Bolhuis, J. P. Hansen, and E. J. Meijer, Phys. Rev. Lett. **85**, 2522 (2000).
[27] P. G. Bolhuis, A. A. Louis, J. P. Hansen, and E. J. Meijer, J. Chem. Phys. **114**, 4296 (2001).
[28] C. Pierleoni, B. Capone, and J. P. Hansen, J. Chem. Phys. **127**, 171102 (2007).
[29] A. Pelissetto, J. Phys.: Condens. Matt. **21**, 115108 (2009).
[30] G. D'Adamo, A. Pelissetto, and C. Pierleoni, Soft Matter **8**, 5151 (2012).
[31] G. D'Adamo, A. Pelissetto, and C. Pierleoni, J. Chem. Phys. **137**, 024901 (2012).
[32] T. Vettorel, G. Besold, and K. Kremer, Soft Matter **6**, 2282 (2010).
[33] A. J. Clark and M. G. Guenza, J. Chem. Phys. **132**, 044902 (2010); A. J. Clark, J. McCarty, I. Y. Lyubimov, and M. G. Guenza, Phys. Rev. Lett. **109**, 168301 (2012).
[34] L. Khounlavong, V. Pryanitsyn, and V. Ganesan, J. Chem. Phys. **133**, 144904 (2010).
[35] R. Chakrabarti and K. S. Schweizer, J. Chem. Phys. **133**, 144905 (2010).
[36] G. Zhang, L. Moreira, T. Stuehn, K. Daoulas, and K. Kremer, ACS Macro Letters **3**, 198 (2014).
[37] P. G. Bolhuis, A. A. Louis, and J. P. Hansen, Phys. Rev. E **64**, 021801 (2001).
[38] A. A. Louis, P. G. Bolhuis, J. P. Hansen, and E. J. Meijer, J. Chem. Phys. **117**, 1893 (2002).
[39] A. A. Louis, P. G. Bolhuis, J. P. Hansen, and E. J. Meijer, J. Chem. Phys. **116**, 10547 (2002).
[40] P. G. Bolhuis, A. A. Louis, and J. P. Hansen, Phys. Rev. Lett. **89**, 128302 (2002).
[41] A. Fortini, P. G. Bolhuis, and M. Dijkstra, J. Chem. Phys. **128**, 024904 (2008).
[42] J. Dzubiella, A. Jusufi, C. N. Likos, C. von Ferber, H. Löwen, J. Stellbrink, J. Allgaier, D. Richter, A. B. Schofield, P. A. Smith, W. C. K. Poon, and P. N. Pusey, Phys. Rev. E **64**, 010401(R) (2001).
[43] J. Dzubiella, C. N. Likos, and H. Löwen, J. Chem. Phys. **116**, 9518 (2002).
[44] R. L. C. Vink, A. Jusufi, J. Dzubiella, and C. N. Likos, Phys. Rev. E **72**, 030401(R) (2005).
[45] P. G. Bolhuis and A. A. Louis, Macromolecules **35**, 1860 (2002).
[46] G. D'Adamo, A. Pelissetto, and C. Pierleoni, J. Chem. Phys. **138**, 234107 (2013).
[47] F. H. Stillinger, H. Sakai, and S. Torquato, J. Chem. Phys. **117**, 288 (2002).
[48] A. A. Louis, J. Phys.: Condens. Matter **14**, 9187 (2002).
[49] P. G. de Gennes, *Scaling Concepts in Polymer Physics* (Cornell University Press, Ithaca, NY, 1979).
[50] N. Clisby, Phys. Rev. Lett. **104**, 55702 (2010).
[51] F. Müller-Plathe, Chem. Phys. Chem. **3**, 754 (2002).
[52] D. Reith, M. Pütz, and F. Müller-Plathe, J. Comp. Chem. **24**, 1624 (2003).
[53] C. Peter and K. Kremer, Soft Matter **5**, 4357 (2009).
[54] H. A. Karimi-Varzaneh and F. Müller-Plathe, in *Multiscale Molecular Methods in Applied Chemistry*, edited by B. Kirchner and J. Vrabec, Top. Curr. Chem. **307** (Springer, Berlin, 2012), p. 295.
[55] E. Brini, E. A. Algaer, P. Ganguly, C. Li, F. Rodriguez-Ropero, N. F. A. van der Vegt, Soft Matter **9**, 2108 (2013).
[56] S. Izvekov and G. A. Voth, J. Phys. Chem B **109**, 2469 (2005); J. Chem. Phys. **123**, 134105 (2005); W. G. Noid, Methods Mol. Biol. **924**, 487 (2013).
[57] W. G. Noid, J. W. Chu, G. S. Ayton, and G. A. Voth, J. Phys. Chem. B **111**, 4116 (2007); J. W. Mullinax and W. G. Noid, Phys. Rev. Lett. **103**, 198104 (2009).
[58] G. D'Adamo, A. Pelissetto, and C. Pierleoni, J. Chem. Phys. **139**, 034901 (2013).
[59] G. D'Adamo, A. Pelissetto, and C. Pierleoni, J. Chem. Phys. **136**, 224905 (2012).
[60] D. J. Ashton and N. B. Wilding, J. Chem. Phys. **140**, 244118 (2014).
[61] In the supplementary material we discuss in detail the Domb-Joyce model we use in the simulations, we present some algorithmic details, and report thermodynamic and structural data in the homogeneous phase. Moreover, we specify the coarse-grained model and, in particular, we provide an explicit parametrization of the polymer-colloid potentials.
[62] C. Domb and G. S. Joyce, J. Phys. C **5**, 956 (1972).
[63] S. Caracciolo, B. M. Mognetti, and A. Pelissetto, J. Chem.

Phys. **125**, 094903 (2006).
[64] P. Belohorec and B.G. Nickel, *Accurate universal and two-parameter model results from a Monte-Carlo renormalization group study*, Guelph University report, 1997 (unpublished).
[65] H. W. Diehl, S. Dietrich, and E. Eisenriegler, Phys. Rev. B **27**, 2937 (1983).
[66] G. D'Adamo, A. Pelissetto, and C. Pierleoni, Mol. Phys. **111**, 3372 (2013).
[67] W. Schommers, Phys. Rev. A **28**, 3599 (1983)
[68] J. P. Hansen and I. McDonald, *Theory of Simple Liquids*, 3rd ed. (Academic Press, Amsterdam, 2006)
[69] Explicit expressions for the virial coefficients that include the flexibility contribution are reported in Ref. 66. Numerically, virial coefficients are computed by using the hit-or-miss algorithm described in Ref. 63. Other methods are described in K. R. S. Shaul, A. J. Schultz, and D. A. Kofke, J. Chem. Phys. **135**, 124101 (2011) and in Ref. 60.
[70] G. J. Fleer, A. M. Skvortsov, and R. Tuinier, Macromol. Theory Simul. **16**, 531 (2007).
[71] J. G. Kirkwood and F. P. Buff, J. Chem. Phys. **19**, 774 (1951).
[72] A. Ben-Naim, *Molecular Physics of Solutions* (Oxford Univ. Press, Oxford, 2006).
[73] In the simulations to determine the phase diagram, Ref. 40 used the Gibbs ensemble with potentials (14).
[74] A. Pelissetto, J. Chem. Phys. **129**, 044901 (2008).
[75] J. L. Lebowitz and J. K. Percus, Phys. Rev. **124**, 1673 (1961).
[76] S. Caracciolo, B. M. Mognetti, and A. Pelissetto, J. Chem. Phys. **125**, 094904 (2006); (erratum) J. Chem. Phys. **126**, 169901 (2007).
[77] T. N. Shendruk, M. Bertrand, H. W. de Haan, J. L. Harden, and G. W. Slater, arXiv:1407.2850
[78] T. Morita, Prog. Theor. Phys. **23** , 829 (1960).
[79] P. Attard, J. Chem. Phys. **94**, 2370 (1991).

Appendix D: Supplementary material: Details on the full-monomer simulations

1. Model and scaling corrections

In order to obtain full-monomer estimates, we consider the three-dimensional lattice Domb-Joyce (DJ) model.[1] In this model the polymer solution is mapped onto N chains of L monomers each on a cubic lattice of linear size M with periodic boundary conditions. Each polymer chain is modelled by a random walk $\{\mathbf{r}_{1A},\ldots,\mathbf{r}_{LA}\}$ with $|\mathbf{r}_{iA}-\mathbf{r}_{i+1,A}|=1$ (we take the lattice spacing as unit of length) and $1\le A\le N$. The Hamiltonian is given by

$$H = \sum_{A=1}^{N}\sum_{1\le i<j\le L}\delta(\mathbf{r}_{iA},\mathbf{r}_{jA}) + \sum_{1\le A<B\le N}\sum_{i=1}^{L}\sum_{j=1}^{L}\delta(\mathbf{r}_{iA},\mathbf{r}_{jB}), \qquad \text{(D1)}$$

where $\delta(\mathbf{r},\mathbf{s})$ is the Kronecker delta. Each configuration is weighted by e^{-wH}, where $w>0$ is a free parameter that plays the role of inverse temperature. This model is similar to the standard lattice self-avoiding walk (SAW) model, which is obtained in the limit $w\to+\infty$. For finite positive w intersections are possible although energetically penalized. For any positive w, this model has the same scaling limit as the SAW model[1] and thus allows us to compute the universal scaling functions that are relevant for polymer solutions under good-solvent conditions. In the absence of colloids, there is a significant advantage in using Domb-Joyce chains instead of SAWs. For SAWs the leading scaling corrections, which decay as $L^{-\Delta}$ ($\Delta=0.528(12)$, Ref. 2), are particularly strong, hence the universal, large–degree-of-polymerization limit is only observed for quite large values of L. Finite-density properties are those that are mostly affected by scaling corrections, and indeed it is very difficult to determine universal thermodynamic properties of polymer solutions for $\Phi\gtrsim 5$ by using lattice SAWs.[3] These difficulties are overcome by using the Domb-Joyce model for a particular value of w,[4–6] $w=0.505838$. For this value of the repulsion parameter, the leading scaling corrections have a negligible amplitude,[4,5] so that scaling corrections decay faster, approximately as $1/L$. As a consequence, scaling results are obtained by using significantly shorter chains. All full-monomer results presented in this paper are obtained by using the optimal model.

It is important to stress that the leading scaling corrections are not related to the lattice nature of the model. Generic continuum models show the same type of scaling corrections as lattice ones, a result that can be proved in the renormalization-group framework. Indeed, using the mapping between polymer models and zero-component spin models,[8], one can show[9] that the leading scaling correction related to the cubic lattice structure scales as $L^{-\omega_{nr}\nu}$, with $\omega_{nr}\approx 2$, hence it is subleading with respect to the one that scales as $L^{-\Delta}$.

The optimal model is particularly convenient computationally, as it allows us to obtain scaling-limit results by considering chains of moderate length. At zero density, simulations with $L=600$ chains provide results that are essentially in the scaling limit (relative differences are less than 1%), without the need of any extrapolation.

The Domb-Joyce model can be extended, including repulsive hard spheres of radius R_c. Their centers are not constrained to belong to the lattice, so that the spheres can move everywhere in continuum space. Colloids interact with the polymers by means of a simple hard-core potential. The interaction potential between a monomer and a colloid is given by $U_m(r)=0$ if $r>R_c$ and $U_m(r)=\infty$ if $r<R_c$.

The nice convergence properties of the Domb-Joyce model do not hold in the presence of repulsive colloids. Indeed, the presence of a hard surface gives rise to new boundary renormalization-group operators.[10] The leading one gives rise to corrections that scale as[10] $L^{-\nu}$, where ν is the Flory exponent (an explicit test of this prediction is presented in the supplementary material of Ref. 7). Because of them, estimates of colloid-polymer properties obtained by using $L=600$ chains are not asymptotic (at the 1% level). For instance, in Table VIII we report the zero-density depletion thickness $\delta_s(0)$ and the quantity δ_1 defined by the expansion[7]

$$\frac{\delta_s(\phi_p)}{\delta_s(0)} = 1+\delta_1\phi_p+O(\phi_p^2), \qquad \text{(D2)}$$

at zero colloidal density. We report the full-monomer scaling results (they are obtained by extrapolating finite-L data, as discussed below) and the estimates obtained by using $L=600$ Domb-Joyce chains. Differences of the order of 2-3% are clearly present. We also report CG estimates. Those corresponding to $L=600$ are obtained by using the model that reproduces the structure of $L=600$ chains, while those labelled "∞" are obtained by using the CG model meant to reproduce the polymer structure in the scaling limit. In Table IX we report the virial combinations defined in Sec. II of the paper. Here we report the results for $L=600$ chains. The corresponding scaling-limit results are reported in Table I of the paper. Again, differences of the order of a few percent between $L=600$ and scaling-limit results are clearly visible.

In order to obtain estimates of full-monomer quantities in the scaling limit, an extrapolation is needed. For this purpose, we proceed as follows. To estimate a universal quantity $f(L)$ in the limit $L\to\infty$, we determine $f(L)$ for $L=L_1=600$ and $L=L_2=2400$. Then, we assume that only the leading scaling correction is relevant, so that the expansion $f(L)=f^*+a/L^\nu$ is accurate for $L\gtrsim 600$. The scaling-limit quantity f^* is then estimated as

$$f^* = \frac{L_1^{-\nu}f(L_2)-L_2^{-\nu}f(L_1)}{L_1^{-\nu}-L_2^{-\nu}}. \qquad \text{(D3)}$$

TABLE VIII: Depletion thickness $\delta_s(0)$ at zero density and first polymer-density correction δ_1, see text for definitions, for $q = 0.5$, 1, and 2. We report full-monomer (FM) results for $L = 600$ Domb-Joyce walks and in the scaling limit ($L = \infty$), and results for the CG model with $n = 1$ and $n = 4$ blobs determined by using the scaling-limit polymer-colloid distribution functions ($L = \infty$) or the distribution functions appropriate for $L = 600$ Domb-Joyce walks.

		$\delta_s(0)/R_c$			δ_1		
L	q	FM	$n = 1$	$n = 4$	FM	$n = 1$	$n = 4$
600	0.5	0.4661(3)	0.46639(3)	0.4666(1)	−1.061(3)	−1.1081(9)	−1.064(5)
∞	0.5	0.474(1)	0.47371(2)	0.4745(1)	−1.05(1)	−1.0924(9)	−1.050(5)
600	1.0	0.8558(4)	0.86209(5)	0.8639(2)	−1.067(2)	−1.1387(4)	−1.097(3)
∞	1.0	0.873(4)	0.86767(5)	0.8764(3)	−1.052(7)	−1.1311(5)	−1.061(4)
600	2.0	1.5053(5)	1.50573(9)	1.5151(3)	−1.0635(10)	−1.1491(3)	−1.103(3)
∞	2.0	1.547(2)	1.54243(9)	1.5487(3)	−1.046(4)	−1.1303(3)	−1.063(3)

TABLE IX: Virial combinations for full-monomer (FM) systems, for the single-blob model ($n = 1$), for the tetramer ($n = 4$), and for the decamer ($n = 10$, model c) model. For the third-virial combinations, we also report the simple-liquid contribution $A^I_{3,\#}$ and the flexibility contribution $A^{\rm fl}_{3,\#}$ (see Ref. 7, App. A, for the definitions): $A_{3,\#} = A^I_{3,\#} + A^{\rm fl}_{3,\#}$. The results are obtained by using Domb-Joyce walks with $L = 600$ monomers and the corresponding CG models (i.e., obtained by using $L = 600$ Domb-Joyce distribution functions as targets). Results in the scaling limit are reported in Table I of the paper.

q	n	$A_{2,cp}$	$A^I_{3,cpp}$	$A^{\rm fl}_{3,cpp}$	$A_{3,ccp}$	$A^I_{3,ccp}$	$A^{\rm fl}_{3,ccp}$	$A_{3,ccp}$
0.5	FM	105.60(6)	732.6(9)	−18.8(4)	714(1)	8522(11)	−124(2)	8400(11)
	1	105.901(6)	693.9(4)	0	693.4(6)	8452(2)	0	8452(2)
	4	105.76(3)	744(2)	−16(1)	729(2)	8557(14)	−119(6)	8439(13)
1	FM	26.77(1)	134.7(2)	−5.8(1)	128.9(2)	355.2(4)	−10.8(1)	345.2(4)
	1	26.796(2)	116.55(6)	0	116.55(6)	331.8(2)	0	331.8(2)
	4	27.126(9)	135.5(4)	−5.0(3)	130.5(4)	356(1)	−10.0(5)	346(1)
	10	26.920(7)	138.5(3)	−6.0(2)	132.4(4)	360.6(6)	−11.0(4)	349.6(6)
2	FM	8.234(5)	26.13(3)	−1.67(2)	24.45(5)	16.60(2)	−0.87(1)	15.73(2)
	1	8.2866(9)	19.16(2)	0	19.16(2)	12.55(2)	0	12.55(2)
	4	8.331(3)	25.1(1)	−1.2(1)	23.9(2)	16.2(2)	−0.7(5)	15.5(2)
	10	8.298(3)	26.7(1)	−1.6(1)	25.0(1)	16.85(9)	−0.91(4)	15.94(9)

2. Algorithmic details

The Domb-Joyce model[1] is very convenient from a computational point of view. Since interactions are soft, the Monte Carlo dynamics for Domb-Joyce chains is quite fast. In the full-monomer simulations we used the algorithm described in Ref. 3, which is very efficient for pure polymer systems, as it allows one to obtain precise results for quite long chains ($L \lesssim 1000$) deep in the semidilute regime.

In order to simulate the system we use several types of moves.

(i) We consider pivot moves[11–14] applied to a single polymer.

(ii) We translate a polymer rigidly by one lattice site. These moves are relevant for the diffusional dynamics of the polymers.

(iii) We consider cut-and-permute (CP) moves.[3,15] In finite-density simulations they represent a nonlocal generalization of the usual reptation moves.

(iv) We consider standard reptation moves.

(v) We consider random translations of the colloids. The average step size is chosen to obtain an average acceptance of 50%.

Let us now discuss the efficiency of the nonlocal polymer moves, extending the discussion of Ref. 3 to the polymer-colloid case. Results for $L = 600$ are reported in Table X. For $q \le 1$ the algorithm is quite efficient. Indeed, the internal structure of the chains is quite rapidly updated by pivot and CP moves. Moreover, chains diffuse quite fast, both because of the rigid translations and

TABLE X: Acceptance ratios $a = N_{\rm acc}/N_{\rm prop}$ ($N_{\rm acc}$ and $N_{\rm prop}$ are the number of accepted and proposed moves, respectively) for pivot moves ($a_{\rm piv}$), translations ($a_{\rm transl}$), and cut-and-permute moves ($a_{\rm cp}$), as a function of q, ϕ_c, and ϕ_p. Results for the optimal Domb-Joyce model: chains with $L = 600$ monomers.

q	ϕ_c	ϕ_p	$a_{\rm piv}$	$a_{\rm transl}$	a_{cp}
0.5	0.2	0.1	0.54100(3)	0.93262(2)	0.38275(3)
1	0.1	0.6	0.40831(4)	0.71848(7)	0.22016(4)
	0.1	0.8	0.36771(5)	0.64211(9)	0.18438(4)
	0.1	1.0	0.33247(6)	0.57291(8)	0.15753(5)
	0.2	0.2	0.43297(4)	0.82749(5)	0.23908(3)
	0.2	0.4	0.38193(3)	0.72371(5)	0.19200(3)
	0.3	0.2	0.35246(6)	0.73942(11)	0.16445(6)
2	0.1	0.6	0.33675(5)	0.64094(10)	0.15767(4)
	0.1	1.0	0.27699(4)	0.50203(11)	0.11924(3)
	0.2	0.4	0.25776(5)	0.55217(12)	0.10510(3)
	0.2	0.8	0.21193(6)	0.40122(15)	0.08308(4)
	0.2	1.0	0.19462(5)	0.34366(10)	0.07555(3)
	0.3	0.2	0.19392(4)	0.45249(16)	0.07274(3)
4	0.3	0.2	0.07832(2)	0.04566(6)	0.02808(2)

of the CP moves. Of course, if L is increased the acceptance rate of the pivot and CP moves decreases, hence the dynamics becomes slower. Note, however, that the change is not large. For $q = 1$, $\phi_c = 0.1$ and $\phi_p = 1.0$ we obtain $a_{\rm piv} = 0.277$ and $a_{\rm cp} = 0.12$ for $L = 2400$ chains. Analogously, for $\phi_c = 0.2$ and $\phi_p = 0.4$ we obtain $a_{\rm piv} = 0.325$ and $a_{\rm cp} = 0.153$ for the same value of L. By increasing L, the acceptance of the translation moves increases, $a_{\rm transl} = 0.67$ and 0.81 for $\phi_c = 0.1$, $\phi_p = 1.0$ and $\phi_c = 0.2$, $\phi_p = 0.4$. This is probably due to the fact that, at fixed ϕ_p, the monomer density decreases as L increases. The improvement in the acceptance, however, does not indicate a better performance of the algorithm. Indeed, translations move the polymer only by one lattice step, while the relevant diffusion length is of the order of the size of the polymer, hence it scales as L^ν. Therefore, even with a larger acceptance, the diffusion dynamics becomes slower.

For $q = 2$ the algorithm worsens somewhat. This is probably due to two different factors. On the one hand, polymers are more compact, as discussed in App. B. On the other hand, the available free space decreases, hence it becomes more difficult to insert a large piece (whose length is of the order of L) of the chain into the system. These problems become more serious for $q = 4$. For $\phi_c = 0.3$ and $\phi_p = 0.2$, the acceptance fractions are small. Moreover, the analysis of the local acceptance fraction, see Ref. 3 for the definition, shows that for $q = 4$ pivot or CP moves are only accepted when the pivot or the cutting point are close to the chain endpoints. Essentially, only local moves are accepted and the CP move is not much better than reptation.

Appendix E: Supplementary material: Explicit expressions for the colloid-blob potentials

We wish now to define in detail the CG model we have considered in this paper. The tetramer CG model used here is defined in Ref. 17 (model 4MB-2). It differs from the model discussed in Ref. 16 because of the presence of an additional angular potential. The expressions of the potentials are given in the supplementary material of Ref. 18 (they are more accurate than those reported in the appendix of Ref. 17). The decamer model is obtained by starting from the tetramer, using the transferability assumption.[17,18]

We report here the colloid-blob potentials for the tetramer. We only give the results appropriate for polymers in the scaling limit. For $q = 0.5$ potentials are parametrized as

$$\beta V_{cp,i}(x, q = 0.5) = a_0 \exp[-b_0 |x - c_0|^{d_0}] + \sum_{i=1}^{3} a_i e^{-((x-c_i)/b_i)^2}. \quad \text{(E1)}$$

This expression parametrizes the data in the range $2.12 < x = r/\hat{R}_g < 7.3$. The coefficients are reported in Table XI. For $q = 1$ and 2 potentials are parametrized as

$$\beta V_{cp,i}(x, q = 1) = \sum_{i=0}^{3} a_i e^{-((x-c_i)/b_i)^2}. \quad \text{(E2)}$$

This expression parametrizes the $q = 1$ potentials in the range $1.01 < x = r/\hat{R}_g < 5.5$ and the $q = 2$ potentials in the range $0.274 < x = r/\hat{R}_g < 4.16$. The coefficients are reported in Table XII for $q = 1$ and in Table XIII for $q = 2$.

TABLE XI: Coefficients parametrizing the colloid-polymer potentials for $q = 0.5$. We report results for the potentials involving the external (Ext) blobs and the internal (Int) blobs.

	i	0	1	2	3
Ext	a_i	9.096478	2.112644	0.012053	0.002480
	b_i	7.674464	0.0476178	0.744283	1.515897
	c_i	2.1	2.1	3.0	4.0
	d_i	0.922204	—	—	—
Int	a_i	7.103179	−0.0402607	−0.0039657	0
	b_i	9.575358	0.536611	0.6702560	0
	c_i	2.099997	2.7	4.0	0
	d_i	1.062409	—	—	—

TABLE XII: Coefficients parametrizing the colloid-polymer potentials for $q = 1$. We report results for the potentials involving the external (Ext) blobs and the internal (Int) blobs.

	i	0	1	2	3
Ext	a_i	4.369300	19.97256	0.257137	−0.250900
	b_i	0.227528	0.531430	1.204911	1.198152
	c_i	0.899934	0.3837873	2.694420	2.703843
Int	a_i	3.900633	8.612210	−0.016251	−0.00361436
	b_i	0.216330	0.400626	0.320438	0.97795073
	c_i	0.899935	0.701953	1.901012	3.24060230

TABLE XIII: Coefficients parametrizing the colloid-polymer potentials for $q = 2$. We report results for the potentials involving the external (Ext) blobs and the internal (Int) blobs.

	i	0	1	2	3
Ext	a_i	0.538768	13.735607	0.002287403	0.007868818
	b_i	0.1832759	0.481442	0.5431964	0.165933
	c_i	0.5056852	0	1.962605	1.1330787
Int	a_i	9.5860832	46.512851	−0.01164300	−0.000896600
	b_i	0.3998641	0.1639868	0.253572	0.488688
	c_i	0.1768134	0	1.459417	2.994538

As a check we compare the virial coefficients computed by using these parametrized expressions for the potentials with those computed by using the numerical potentials obtained as output of the Iterative Boltzmann Inversion procedure. For $q = 0.5$ we find a relative difference of 1.4%, 0.9%, 2.0% for $A_{2,cp}$, $A_{3,cpp}$, and $A_{3,ccp}$. For $q = 1$ the relative difference is significantly smaller: 0.1%, 0.6%, and 0.1%, respectively. For $q = 2$, we obtain 1.8%, 1.1%, and 0.7% for the same quantities, respectively. All results presented in the paper were obtained by using the numerical potentials.

Appendix F: Supplementary material: Intramolecular structure

In Secs. V and VI of the text, we discussed how the CG model reproduces the intramolecular structure of the full-monomer system. In particular, we focused on the intramolecular distribution function of the n-blob CGR of the polymer model, defined by

$$g_{\text{intra},n}(\mathbf{r}) = \frac{2\hat{R}_g^3}{n(n-1)} \sum_{i<j} \langle \delta(\mathbf{r} - \mathbf{s}_i - \mathbf{s}_j) \rangle \,, \qquad \text{(F1)}$$

TABLE XIV: Radius of gyration $R_{g,b}$ of the CGR of the polymer model with $n = 4$ and $n = 10$ blobs (CGR-4 and CGR-10, respectively). Results appropriate for $L = 600$ Domb-Joyce chains. We also report the radius of gyration for the tetramer (CG-4) and the decamer (CG-10) models.

q	ϕ_c	ϕ_p	CGR-4	CG-4	CGR-10	CG-10
1	0.1	0.6	0.84873(3)	0.85304(3)	0.92086(2)	0.91702(6)
	0.1	0.8	0.84121(4)	0.84724(4)	0.91324(2)	
	0.2	0.2	0.84120(4)	0.84132(8)	0.91358(2)	
	0.2	0.4	0.83281(2)	0.83408(4)	0.90507(1)	0.89978(4)
	0.3	0.2	0.81149(6)	0.80837(6)	0.88400(3)	0.87651(3)
2	0.1	0.6	0.83427(5)	0.84037(4)	0.90603(2)	0.90003(4)
	0.1	1.0	0.82117(5)	0.83179(5)	0.89268(2)	0.88632(4)
	0.2	0.4	0.80087(6)	0.80682(5)	0.87233(3)	0.86106(4)
	0.2	0.8	0.78822(8)	0.80191(5)	0.85939(3)	0.84921(4)
	0.3	0.2	0.75696(7)	0.76645(6)	0.82816(3)	0.81109(3)

where $\mathbf{s}_i$ are the blob positions. For large L, $g_{\text{intra},n}(\mathbf{r})$ is a universal function of $\mathbf{b} = \mathbf{r}/\hat{R}_g$, where $\hat{R}_g$ is the zero-density radius of gyration. At zero polymer and colloid density, $g_{\text{intra},n}(\mathbf{r})$ is completely consistent[16] with the tetramer and decamer distribution functions, confirming the accuracy of the inversione procedure (tetramer case) and of the transferability assumption (decamer). The same good agreement is observed at the set of state points we have considered in Sec. V of the paper, which belong to the homogeneous phase and are not too close to the binodal, see, e.g., Fig. 7 in the main paper. A more quantitative check can be performed by considering the radius of gyration of the CGR representation of the polymer, defined by

$$R_{g,b}^2 = \frac{1}{2n^2} \sum_{i,j=1}^{n} (\mathbf{s}_i - \mathbf{s}_j)^2. \qquad \text{(F2)}$$

Such a quantity is always smaller than R_g, since

$$R_g^2 = R_{g,b}^2 + \frac{1}{n} \sum_{i=1}^{n} r_{g,i}^2, \qquad \text{(F3)}$$

where $r_{g,i}$ is the radius of gyration of i-th blob (m is the number of monomers belonging to each blob):

$$r_{g,i}^2 = \frac{1}{2m^2} \sum_{k,l=m(i-1)+1}^{mi} (\mathbf{r}_k - \mathbf{r}_l)^2. \qquad \text{(F4)}$$

The ratios $R_{g,b}^2/R_g^2$ and $r_{g,i}^2/R_g^2$ of their averages over the polymer configurations are universal, hence independent of the nature of the underlying polymer model as long as L is large enough. The quantity $R_{g,b}/\hat{R}_g$ can be directly compared with the radius of gyration of the correspond-

ing CG model. Estimates are reported in Ref. XIV. Differences are always very small, for both $q = 1$ and $q = 2$, indicating that the CG model correctly reproduces the intramolecular polymer structure at the coarse-grained level.

Appendix G: Supplementary material: Tables of thermodynamic results

In this Section we report extensive tables of thermodynamic data for several state points in the homogeneous phase for $q = 0.5$, $q = 1$, and $q = 2$. We report full-monomer results (only for $q = 1$ and $q = 2$), GFVT results, and estimates obtained in the CG models with different number of blobs. Note that full-monomer results have been obtained by using Domb-Joyce walks with $L = 600$ monomers, without performing any extrapolation, hence results are expected to differ by a few percent from the scaling, universal estimates. To be consistent, the CG models we consider in this section have been obtained by using $L = 600$ Domb-Joyce distribution functions as targets. Therefore, differences between CG and full-monomer results are only the result of the inaccuracy of the CG procedure. On the other hand, GFVT results are obtained by using scaling-limit results for $K_p(\phi_p)$ and for the depletion thickness, hence they should be rather compared with CG and full-monomer scaling-limit results. As we already mentioned in Sec. D 2 however, the difference between scaling and $L = 600$ results is quite small (a few per cent). In particular, it is significantly smaller than the observed discrepancies between GFVT and full-monomer predictions, which are therefore mostly due to the approximate nature of the theory.

Details on the full-monomer runs are reported in Table XV. Results for $q = 0.5$ are reported in Tables XVI, XVII, and XVIII. For this value of q, tetramer results should be accurate and also GFVT should be reliable, hence we can use the latter to estimate the boundary of the homogeneous phase. For $\phi_c = 0.1$, phase separation occurs for $\phi_p \gtrsim 0.5$, hence the state point $\phi_c = 0.1$ and $\phi_p = 0.4$ is not far from the binodal. In this case, GFVT gives results which do not differ significantly from the tetramer ones. Note also that GFVT is more accurate than the single-blob model. For $\phi_c = 0.3$ and $\phi_p = 0.1$, GFVT, single-blob and tetramer results are close. For $\phi_c = 0.3$ and $\phi_p = 0.2$, GFVT predicts phase separation. It is not clear whether phase separation also occurs in the single-blob and/or in the tetramer model (the results we report are obtained in canonical simulations). Hints of phase separation are provided by the quite large value of $S_{pp,0}$.

Thermodynamic results for $q = 1$ and $\phi_c = 0.1$ are reported in Tables XIX, XX, and XXI. For this value of ϕ_p, the tetramer estimates are always consistent with the full-monomer ones, confirming its accuracy for $q = 1$. Single-blob results differ instead significantly. Note, in particular, that $|S_{\alpha\beta,0}|$ is relatively small and does not change significantly as ϕ_p is increased from 0.8 to 1.0, a behavior which indicates that the single-blob model undergoes phase separation, assuming it occurs, only for $\phi_p \gg 1$. GFVT predicts phase separation for $\phi_p \approx 0.72$, which is consistent with the somewhat large value of $S_{pp,0}$ for $\phi_p = 0.6$. For this value of ϕ_p, the GFVT estimates of $|S_{\alpha\beta,0}|$ and of $1/g''$ are not consistent with the full-monomer ones. Differences are instead significantly smaller in the case of K_p, K_c, and $\beta R_c^3/\chi_T$.

The results for $\phi_c = 0.2$, reported in Tables XXII and XXIII, confirm what observed for $\phi_c = 0.1$. The tetramer

TABLE XV: Details on the full-monomer simulations of $L = 600$ Domb-Joyce chains: N_c and N_p are the number of colloids and polymers, respectively, M the linear size of the cubic box, $\hat{R}_g$ the zero-density radius of gyration, and $N_{\rm it}$ the number of iterations. Each iteration consists in one pivot, one cut-and-permute, and one polymer translation applied sequentially to each polymer, $60N_p$ reptations, and $N_pN_c/5$ colloid translations. More precisely, after applying the three nonlocal moves to a given polymer, we perform one reptation move on 60 randomly chosen polymers and translate $N_c/5$ randomly chosen colloids.

q	ϕ_c	ϕ_p	N_c	N_p	M	$M/\hat{R}_g$	$N_{\rm it}/10^3$
1	0.1	0.6	111	664	256	16.7	250
	0.1	0.8	111	885	256	16.7	200
	0.1	1.0	111	1106	256	16.7	200
	0.2	0.2	221	221	256	16.7	500
	0.2	0.2	1769	1769	512	33.3	150
	0.2	0.4	221	442	256	16.7	1000
	0.3	0.2	332	221	256	16.7	500
2	0.1	0.6	885	664	256	16.7	150
	0.1	1.0	885	1106	256	16.7	100
	0.2	0.4	1769	442	256	16.7	250
	0.2	0.8	1769	885	256	16.7	150
	0.3	0.2	2654	221	256	16.7	300

TABLE XVI: Estimates of several thermodynamic quantities for $q = 0.5$, $\phi_c = 0.1$, $\phi_p = 0.4$. Definitions are given in App. A of the paper. We report GFVT estimates and results obtained in CG models with $n = 1$ and $n = 4$ blobs.

	GFVT	$n = 1$	$n = 4$
$S_{pp,0}$	3.147	2.76(1)	3.5(2)
$S_{cp,0}$	−1.724	−1.57(2)	−2.0(1)
$S_{cc,0}$	1.0781	1.05(2)	1.36(8)
K_p	3.295	3.068(6)	3.28(2)
K_c	30.74	27.0(1)	28.9(2)
$\frac{\beta R_c^3}{\chi_T}$	3.251	2.99(6)	3.20(2)
$1/g''$	0.051	0.0480(7)	0.062(4)

TABLE XVII: Estimates of several thermodynamic quantities for $q = 0.5$, $\phi_c = 0.3$, $\phi_p = 0.1$. Definitions are given in App. A of the paper. We report GFVT estimates and results obtained in CG models with $n = 1$ and $n = 4$ blobs.

	GFVT	$n = 1$	$n = 4$
$S_{pp,0}$	2.69	2.20(1)	2.33(3)
$S_{cp,0}$	−0.70	−0.55(4)	−0.59(1)
$S_{cc,0}$	0.24	0.197(1)	0.208(3)
K_p	4.318	4.01(1)	4.26(1)
K_c	24.69	23.30(7)	24.6(1)
$\frac{\beta R_c^3}{\chi_T}$	2.59	2.43(6)	2.58(1)
$1/g''$	0.30	0.244(2)	0.261(4)

TABLE XVIII: Estimates of several thermodynamic quantities for $q = 0.5$, $\phi_c = 0.3$, $\phi_p = 0.2$. Definitions are given in App. A of the paper. We report results obtained in CG models with $n = 1$ and $n = 4$ blobs. We do not report the GFVT estimates, since this point belongs to the region in which GFVT predicts phase separation.

	$n = 1$	$n = 4$
$S_{pp,0}$	4.78(6)	6.19(3)
$S_{cp,0}$	−1.32(2)	−1.74(1)
$S_{cc,0}$	0.408(6)	0.43(3)
K_p	4.69(1)	5.20(3)
K_c	37.4(1)	41.5(2)
$\frac{\beta R_c^3}{\chi_T}$	4.47(1)	4.96(2)
$1/g''$	0.274(4)	0.36(2)

model accurately reproduces the full-monomer results. GFVT predicts a critical point for $\phi_{c,\mathrm{crit}} = 0.178$ and $\phi_{p,\mathrm{crit}} = 0.474$ (this explains the large estimates of the zero-momentum structure factors in Table XXIII). Results for $\phi_c = 0.3$ are reported in Table XXIV. While tetramer and decamer results are consistent with the full-monomer ones, GFVT and single-blob results differ somewhat. As observed before, GFVT appears to be more accurate than the single-blob model.

Results for $q = 2$ are reported in Tables XXV, XXVI, XXVII, XXVIII, and XXIX. Comparing the full-monomer and the tetramer results, we find that CG model is reasonably accurate except for $\phi_c = 0.2$ and $\phi_p = 0.8$. This state point, however, is not too far from the full-monomer critical point, $\phi_{c,\mathrm{crit}} \approx 0.19$, $\phi_{p,\mathrm{crit}} \approx 1.18$, which was estimated in Ref. 19. Therefore, we conclude that the tetramer is reasonably accurate in the homogeneous phase also for $q = 2$, except close to the critical point. No differences are observed instead between decamer and full-monomenr results. As expected, GFVT and single-blob results differ significantly from the correct ones.

TABLE XIX: Estimates of several thermodynamic quantities for $q = 1$, $\phi_c = 0.1$, $\phi_p = 0.6$. Definitions are given in App. A of the paper. We report full-monomer (FM), GFVT estimates, and results obtained in CG models with $n = 1$, $n = 4$, and $n = 10$ blobs.

	FM	GFVT	$n = 1$	$n = 4$	$n = 10$
$S_{pp,0}$	1.46(4)	2.352	1.25(2)	1.39(4)	1.41(4)
$S_{cp,0}$	−1.20(4)	−2.030	−1.00(2)	−1.13(4)	−1.16(4)
$S_{cc,0}$	1.22(4)	1.985	1.06(2)	1.15(4)	1.19(4)
K_p	5.11(6)	5.14	4.32(2)	4.98(3)	5.13(2)
K_c	13.1(2)	13.39	10.85(7)	12.85(8)	13.15(6)
$\frac{\beta R_c^3}{\chi_T}$	1.05(1)	1.0564	0.887(5)	1.021(5)	1.049(4)
$1/g''$	0.258(8)	0.4235	0.219(4)	0.2415(83)	0.249(8)
$\beta\mu_p^{(\mathrm{exc})}$		3.161	2.8586(5)	3.117(2)	3.17(2)

TABLE XX: Estimates of several thermodynamic quantities for $q = 1$, $\phi_c = 0.1$, $\phi_p = 0.8$. Definitions are given in App. A of the paper. We report full-monomer (FM) estimates and results obtained in CG models with $n = 1$ and $n = 4$ blobs. We do not report the GFVT estimates, since this point belongs to the region in which GFVT predicts phase separation. For $\phi_c = 0.1$, GFVT predicts the system to be homogeneous only up to $\phi_p \approx 0.72$.

	FM	$n = 1$	$n = 4$
$S_{pp,0}$	1.92(9)	1.34(2)	1.86(10)
$S_{cp,0}$	−1.72(9)	−1.16(2)	−1.66(10)
$S_{cc,0}$	1.72(9)	1.25(3)	1.68(10)
K_p	6.45(8)	5.08(3)	6.10(4)
K_c	18.7(2)	14.19(8)	17.7(2)
$\frac{\beta R_c^3}{\chi_T}$	1.68(2)	1.309(7)	1.59(1)
$1/g''$	0.28(1)	0.196(4)	0.27(2)
$\beta\mu_p^{(\mathrm{exc})}$		3.5692(5)	3.978(4)

TABLE XXI: Estimates of several thermodynamic quantities for $q = 1$, $\phi_c = 0.1$, $\phi_p = 1.0$. Definitions are given in App. A of the paper. We report full-monomer (FM) estimates and results obtained in CG models with $n = 1$ and $n = 4$ blobs. We do not report the GFVT estimates, since this point belongs to the region in which GFVT predicts phase separation. For $\phi_c = 0.1$, GFVT predicts the system to be homogeneous only up to $\phi_p \approx 0.72$.

	FM	$n = 1$	$n = 4$
$S_{pp,0}$	3.08(25)	1.36(4)	2.97(25)
$S_{cp,0}$	−2.95(25)	−1.25(4)	−2.82(25)
$S_{cc,0}$	2.98(25)	1.36(4)	2.85(25)
K_p	7.6(1)	5.90(3)	7.27(4)
K_c	24.1(4)	17.82(9)	23.1(2)
$\frac{\beta R_c^3}{\chi_T}$	2.40(4)	1.833(9)	2.3(2)
$1/g''$	0.39(3)	0.172(5)	0.37(4)
$\beta\mu_p^{(\mathrm{exc})}$		4.2796(5)	4.862(5)

TABLE XXII: Estimates of several thermodynamic quantities for $q = 1$, $\phi_c = 0.2$, $\phi_p = 0.2$. Definitions are given in App. A of the paper. We report full-monomer (FM), GFVT estimates, and results obtained in CG models with $n = 1$ and $n = 4$ blobs.

	FM	GFVT	$n = 1$	$n = 4$
$S_{pp,0}$	1.48(10)	1.60	1.44(1)	1.54(2)
$S_{cp,0}$	−0.66(5)	−0.76	−0.619(8)	−0.691(1)
$S_{cc,0}$	0.44(2)	0.53	0.428(5)	0.461(8)
K_p	5.01(6)	4.92	4.42(3)	4.95(3)
K_c	9.72(5)	9.02	8.73(6)	9.59(6)
$\frac{\beta R_c^3}{\chi_T}$	0.703(5)	0.666	0.63(4)	0.694(5)
$1/g''$	0.41(3)	0.46	0.389(4)	0.423(7)
$\beta\mu_p^{(\mathrm{exc})}$		2.78	2.6064(6)	2.763(3)

TABLE XXIII: Estimates of several thermodynamic quantities for $q = 1$, $\phi_c = 0.2$, $\phi_p = 0.4$. Definitions are given in App. A of the paper. We report full-monomer (FM), GFVT estimates, and results obtained in CG models with $n = 1$, $n = 4$, and $n = 10$ blobs. Within GFVT, this state point is essentially on top of the fluid-fluid binodal and not far from the GFVT critical point $\phi_{c,\mathrm{crit}} = 0.178$, $\phi_{p,\mathrm{crit}} = 0.474$.

	FM	GFVT	$n = 1$	$n = 4$	$n = 10$
$S_{pp,0}$	2.68(7)	12.2	2.00(3)	2.62(5)	2.63(3)
$S_{cp,0}$	−1.49(4)	−7.56	−1.07(2)	−1.46(30)	−1.48(2)
$S_{cc,0}$	0.95(2)	4.80	0.70(1)	0.92(2)	0.94(1)
K_p	6.51(2)	6.67	5.37(3)	6.45(3)	6.63(2)
K_c	15.60(5)	15.0	12.94(8)	15.45(7)	15.75(4)
$\frac{\beta R_c^3}{\chi_T}$	1.366(4)	1.36	1.131(6)	1.354(1)	1.385(3)
$1/g''$	0.65(2)	3.20	0.476(8)	0.64(1)	0.644(9)
$\beta\mu_p^{(\mathrm{exc})}$		3.827	3.3926(7)	3.746(3)	3.77(1)

TABLE XXIV: Estimates of several thermodynamic quantities for $q = 1$, $\phi_c = 0.3$, $\phi_p = 0.2$. Definitions are given in App. A of the paper. We report full-monomer (FM), GFVT estimates, and results obtained in CG models with $n = 1$, $n = 4$, and $n = 10$ blobs.

	FM	GFVT	$n = 1$	$n = 4$	$n = 10$
$S_{pp,0}$	2.37(9)	1.72	1.69(3)	2.25(5)	2.47(5)
$S_{cp,0}$	−0.83(3)	−0.65	−0.534(1)	−0.785(20)	−0.87(2)
$S_{cc,0}$	0.36(1)	0.32	0.247(4)	0.341(8)	0.375(8)
K_p	8.60(3)	8.50	6.88(5)	8.53(5)	8.70(4)
K_c	19.00(7)	17.57	16.2(1)	18.9(1)	19.19(8)
$\frac{\beta R_c^3}{\chi_T}$	1.772(6)	1.625	1.49(1)	1.76(1)	1.790(8)
$1/g''$	0.57(2)	0.404	0.392(8)	0.541(1)	0.60(2)
$\beta\mu_p^{(\mathrm{exc})}$		4.48	4.0829(8)	4.529(5)	4.58(2)

TABLE XXV: Estimates of several thermodynamic quantities for $q = 2$, $\phi_c = 0.1$, $\phi_p = 0.6$. Definitions are given in App. A of the paper. We report full-monomer (FM), GFVT estimates, and results obtained in CG models with $n = 1$, $n = 4$, and $n = 10$ blobs.

	FM	GFVT	$n = 1$	$n = 4$	$n = 10$
$S_{pp,0}$	0.75(3)	0.79	0.652(2)	0.737(9)	0.736(8)
$S_{cp,0}$	−0.69(3)	−0.80	−0.512(2)	−0.66(1)	−0.679(9)
$S_{cc,0}$	0.99(3)	1.21	0.808(4)	0.95(1)	0.97(1)
K_p	6.81(6)	6.86	5.29(7)	6.55(3)	6.90(2)
K_c	5.13(3)	4.77	4.14(8)	5.00(3)	5.20(2)
$\frac{\beta R_c^3}{\chi_T}$	0.245(2)	0.237	0.1935(3)	0.237(1)	0.248(1)
$1/g''$	0.38(2)	0.432	0.300(1)	0.364(5)	0.370(4)
$\beta\mu_p^{(\mathrm{exc})}$		4.52	3.8541(3)	4.402(2)	4.46(3)

TABLE XXVI: Estimates of several thermodynamic quantities for $q = 2$, $\phi_c = 0.1$, $\phi_p = 1.0$. Definitions are given in App. A of the paper. We report full-monomer (FM), GFVT estimates, and results obtained in CG models with $n = 1$, $n = 4$, and $n = 10$ blobs. Within the GFVT approximation, this point is not too far from the binodal (for $\phi_c = 0.1$ the system is homogeneeous up to $\phi_p \approx 1.3$) and the critical point $\phi_{c,\mathrm{crit}} = 0.115$, $\phi_{p,\mathrm{crit}} = 1.205$.

	FM	GFVT	$n = 1$	$n = 4$	$n = 10$
$S_{pp,0}$	0.71(4)	1.47	0.522(2)	0.706(20)	0.71(2)
$S_{cp,0}$	−0.84(5)	−2.00	−0.516(4)	−0.796(25)	−0.83(2)
$S_{cc,0}$	1.28(6)	3.07	0.895(6)	1.207(35)	1.27(3)
K_p	9.8(1)	9.75	6.74(1)	8.78(6)	9.62(5)
K_c	7.94(7)	7.43	5.46(1)	7.30(6)	7.88(4)
$\frac{\beta R_c^3}{\chi_T}$	0.481(5)	0.469	0.332(6)	0.436(3)	0.476(2)
$1/g''$	0.458(25)	1.07	0.307(2)	0.44(1)	0.460(1)
$\beta\mu_p^{(\mathrm{exc})}$		6.52	5.2262(4)	6.120(5)	6.42(8)

TABLE XXVII: Estimates of several thermodynamic quantities for $q = 2$, $\phi_c = 0.2$, $\phi_p = 0.4$. Definitions are given in App. A of the paper. We report full-monomer (FM), GFVT estimates, and results obtained in CG models with $n = 1$, $n = 4$, and $n = 10$ blobs.

	FM	GFVT	$n = 1$	$n = 4$	$n = 10$
$S_{pp,0}$	1.27(8)	0.656	0.86(1)	1.22(4)	1.33(2)
$S_{cp,0}$	−0.83(5)	−0.415	−0.43(1)	−0.763(25)	−0.87(2)
$S_{cc,0}$	0.71(3)	0.45	0.42(1)	0.65(2)	0.74(1)
K_p	11.35(7)	10.56	7.36(4)	10.5(1)	11.30(7)
K_c	8.07(4)	7.14	6.20(7)	7.77(8)	8.05(5)
$\frac{\beta R_c^3}{\chi_T}$	0.521(3)	0.467	0.383(3)	0.495(5)	0.520(3)
$1/g''$	0.29(2)	0.151	0.179(3)	0.274(9)	0.306(3)
$\beta\mu_p^{(\mathrm{exc})}$		6.58	5.519(1)	6.713(5)	6.97(3)

TABLE XXVIII: Estimates of several thermodynamic quantities for $q = 2$, $\phi_c = 0.2$, $\phi_p = 0.8$. Definitions are given in App. A of the paper. We report full-monomer (FM), GFVT estimates, and results obtained in CG models with $n = 1$, $n = 4$, and $n = 10$ blobs.

	FM	GFVT	$n = 1$	$n = 4$	$n = 10$
$S_{pp,0}$	2.6(3)	1.43	0.701(8)	1.55(9)	2.6(1)
$S_{cp,0}$	−2.2(3)	−1.33	−0.472(8)	−1.25(8)	−2.2(1)
$S_{cc,0}$	2.0(2)	1.39	0.510(9)	1.15(7)	2.0(1)
K_p	15.2(2)	15.27	8.79(2)	13.2(2)	14.8(1)
K_c	12.2(1)	11.05	7.72(4)	11.0(2)	11.9(1)
$\frac{\beta R_c^3}{\chi_T}$	0.946(9)	0.892	0.579(2)	0.84(1)	1.00(5)
$1/g''$	1.0(1)	0.593	0.241(4)	0.58(4)	1.00(5)
$\beta\mu_p^{(\mathrm{exc})}$		9.29	6.920(7)	8.81(1)	9.42(5)

TABLE XXIX: Estimates of several thermodynamic quantities for $q = 2$, $\phi_c = 0.3$, $\phi_p = 0.2$. Definitions are given in App. A of the paper. We report full-monomer (FM), GFVT estimates, and results obtained in CG models with $n = 1$, $n = 4$, and $n = 10$ blobs.

	FM	GFVT	$n = 1$	$n = 4$	$n = 10$
$S_{pp,0}$	1.5(1)	0.48	0.863(4)	1.38(4)	1.58(3)
$S_{cp,0}$	−0.60(4)	−0.147	−0.197(1)	−0.50(2)	−0.62(1)
$S_{cc,0}$	0.319(15)	0.136	0.143(2)	0.263(7)	0.326(5)
K_p	18.74(7)	15.01	9.8(1)	16.6(2)	18.6(1)
K_c	13.29(4)	12.07	10.9(2)	12.8(1)	13.22(5)
$\frac{\beta R_c^3}{\chi_T}$	1.063(3)	0.954	0.84(1)	1.015(10)	1.057(4)
$1/g''$	0.124(8)	0.037	0.0648(4)	0.111(4)	0.128(2)
$\beta\mu_p^{(\mathrm{exc})}$		8.58	7.4151(7)	9.778(8)	10.27(2)

* Electronic address: giuseppe.dadamo@sissa.it
† Electronic address: andrea.pelissetto@roma1.infn.it
‡ Electronic address: carlo.pierleoni@aquila.infn.it

[1] C. Domb and G. S. Joyce, J. Phys. C **5**, 956 (1972).
[2] N. Clisby, Phys. Rev. Lett. **104**, 55702 (2010).
[3] A. Pelissetto, J. Chem. Phys. **129**, 044901 (2008).
[4] P. Belohorec and B.G. Nickel, *Accurate universal and two-parameter model results from a Monte-Carlo renormalization group study*, Guelph University report, 1997 (unpublished).
[5] S. Caracciolo, B. M. Mognetti, and A. Pelissetto, J. Chem. Phys. **125**, 094903 (2006).
[6] Simulations have been performed at $w = 0.505838$, as in our previous works. This value is optimal within errors. The optimal value w^* at which the leading scaling corrections are absent was estimated in Ref. 5, obtaining $w^* = 0.48 \pm 0.02$.
[7] G. D'Adamo, A. Pelissetto, and C. Pierleoni, Mol. Phys. **111**, 3372 (2013).
[8] P. G. de Gennes, *Scaling Concepts in Polymer Physics* (Cornell University Press, Ithaca, NY, 1979).
[9] M. Campostrini, A. Pelissetto, P. Rossi, and E. Vicari, Phys. Rev. E **57**, 184 (1998).
[10] H. W. Diehl, S. Dietrich, and E. Eisenriegler, Phys. Rev. B **27**, 2937 (1983).
[11] M. Lal, Molec. Phys. **17**, 57 (1969).
[12] B. MacDonald, N. Jan, D. L. Hunter and M. O. Steinitz, J. Phys. A **18**, 2627 (1985).
[13] N. Madras and A. D. Sokal, J. Stat. Phys. **50**, 109 (1988).
[14] A. D. Sokal, in *Monte Carlo and Molecular Dynamics Simulations in Polymer Science*, edited by K. Binder (Oxford Univ. Press, Oxford, 1995).
[15] M. S. Causo, J. Stat. Phys. **108**, 247 (2002).
[16] G. D'Adamo, A. Pelissetto, and C. Pierleoni, Soft Matter **8**, 5151 (2012).
[17] G. D'Adamo, A. Pelissetto, and C. Pierleoni, J. Chem. Phys. **137**, 024901 (2012).
[18] G. D'Adamo, A. Pelissetto, and C. Pierleoni, J. Chem. Phys. **139**, 034901 (2013).
[19] G. D'Adamo, A. Pelissetto, and C. Pierleoni, J. Chem. Phys. **141**, 024902 (2014).